ILC1 drive intestinal epithelial and matrix remodelling

Geraldine M. Jowett[1,2,3,4], Michael D. A. Norman*[1], Tracy T. L. Yu*[1], Patricia Rosell Arévalo[2], Dominique Hoogland[5], Suzette Lust[1], Emily Read[2,3], Eva Hamrud[1,3,4], Nick J. Walters[6], Umar Niazi[7], Matthew Wai Heng Chung[2,3,4], Daniele Marciano[1], Omer Serhan Omer[8,9], Tomasz Zabinski[2], Davide Danovi[4], Graham M. Lord[10], Jöns Hilborn[11], Nicholas D. Evans[12], Cécile A. Dreiss[13], Laurent Bozec[14], Oommen P. Oommen[15], Christian D. Lorenz[16], Ricardo M.P. da Silva[1,17], Joana F. Neves†[#2], Eileen Gentleman†[#1]

[1] Centre for Craniofacial and Regenerative Biology, King's College London, London SE1 9RT, UK
[2] Centre for Host Microbiome Interactions, King's College London, London, SE1 9RT, UK
[3] Wellcome Trust Cell Therapies and Regenerative Medicine PhD programme
[4] Centre for Stem Cells & Regenerative Medicine, King's College London, London, SE1 9RT, UK
[5] Department of Chemistry, King's College London, London SE1 1DB, UK
[6] BioMediTech, Tampere University, 33014 Tampereen yliopisto, Finland, and Natural Resources Institute Finland, 00790 Helsinki, Finland
[7] Guy's and St Thomas' National Health Service Foundation Trust and King's College London National Institute for Health Research Biomedical Research Centre Translational Bioinformatics Platform, Guy's Hospital, London, UK
[8] School of Immunology and Microbial Sciences, King's College London, London, UK
[9] Department of Gastroenterology, Guy's and St Thomas' Hospitals NHS Trust, London, UK
[10] Faculty of Biology, Medicine and Health, University of Manchester, M13 9NT, UK
[11] Department of Chemistry, Ångström Laboratory, Uppsala University, Uppsala 75121, Sweden
[12] Bone and Joint Research Group, Centre for Human Development, Stem Cells and Regeneration, Human Development and Health, Institute of Developmental Sciences, University of Southampton, Southampton, UK.
[13] Institute of Pharmaceutical Science, Franklin-Wilkins Building, King's College London, London SE1 9NH, UK
[14] Faculty of Dentistry, University of Toronto, Toronto, Canada
[15] Bioengineering and Nanomedicine Lab, Faculty of Medicine and Health Technology, Tampere University, 33720 Tampere, Finland
[16] Department of Physics, King's College London, London WC2R 2LS, UK
[17] i3S - Instituto de Investigação e Inovação em Saúde and INEB - Instituto de Engenharia Biomédica, Universidade do Porto, Rua Alfredo Allen, 208, 4200 - 135 Porto, Portugal

*These two authors contributed equally; listed in alphabetical order.
#These two authors contributed equally.
†To whom correspondence should be addressed: eileen.gentleman@kcl.ac.uk or joana.pereira_das_neves@kcl.ac.uk

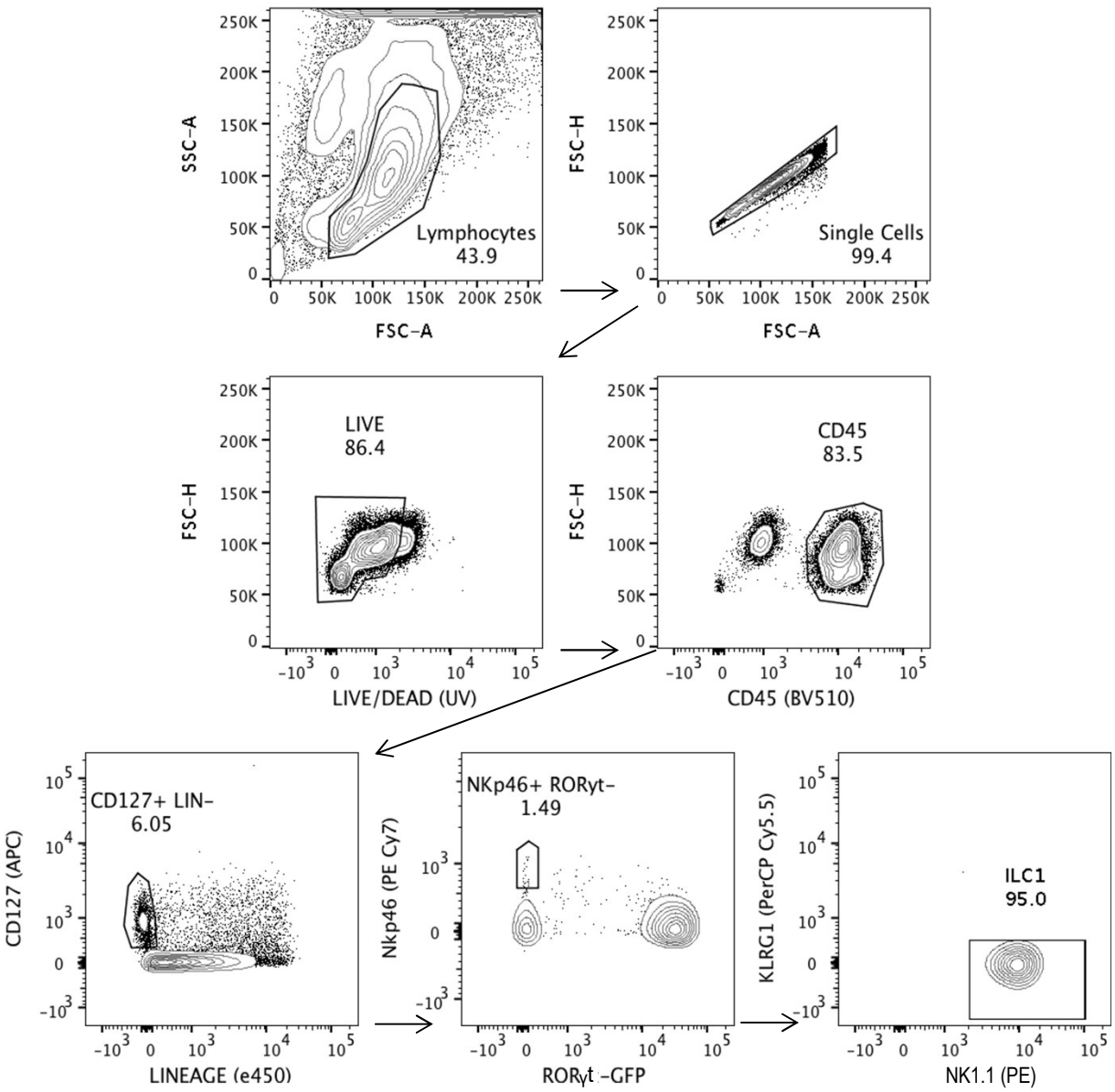

Supplementary Figure 1. FACS gating strategy for the purification of ILC1 from the small intestinal lamina propria of female RORγt-GFP reporter mice

Gates were set based on relevant fluorescent minus one (FMO), used for Lineage (FITC), CD127 (APC), and NKp46 (PE Cy7). ILC1 were defined as single cells, live, CD127^{+}, Lineage (CD3, CD5, CD19, Ly6G)$^{-}$, RORγt^{-}, NKp46^{+}, KLRG1^{-} and NK1.1^{+}.

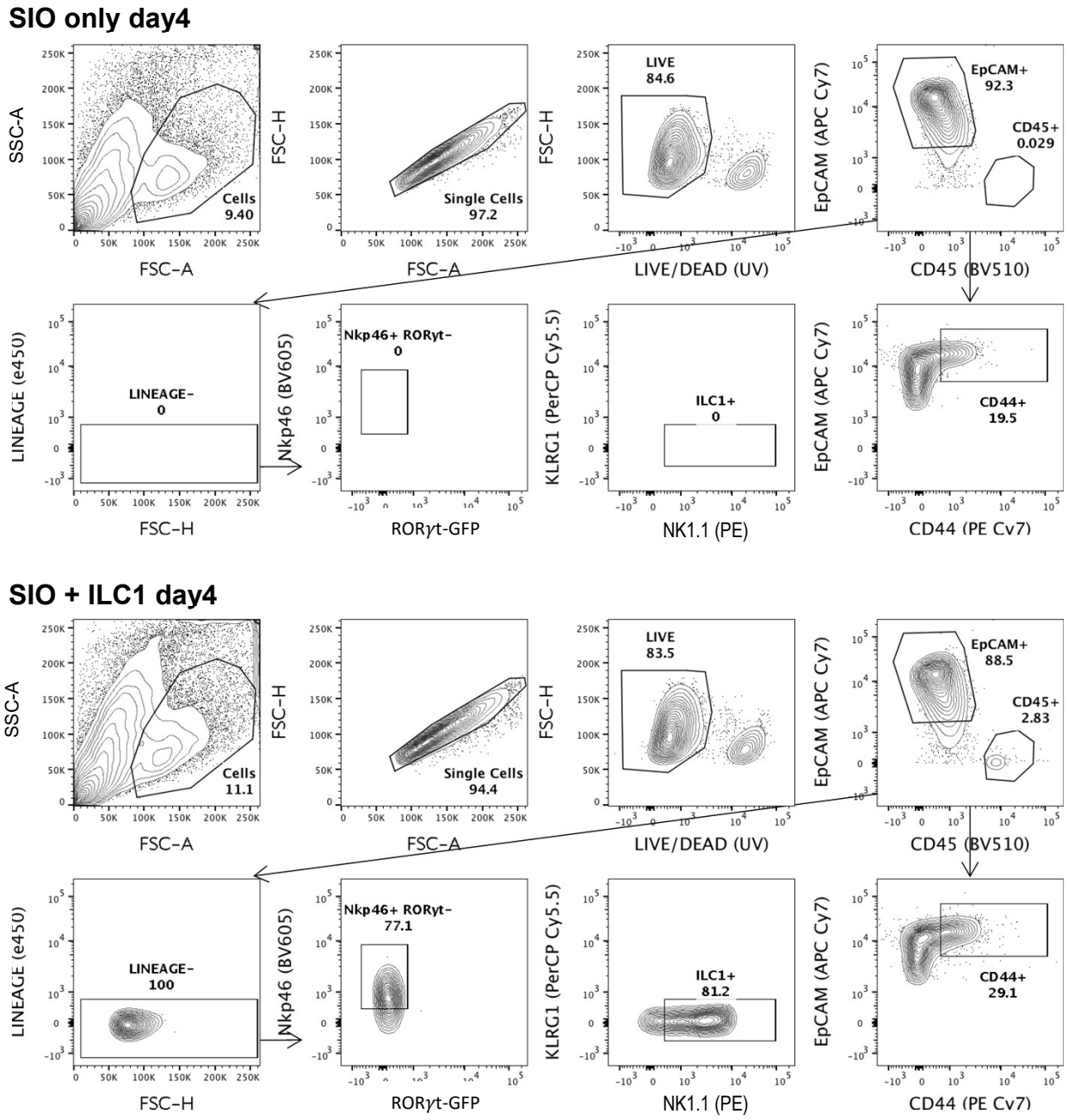

Supplementary Figure 2. Gating strategy for FACS isolation of ILC1 and IEC from co-cultures
FACS gating strategy for dissociated ILC1-SIO co-cultures, sorting epithelial cells (single cells, live, $EpCAM^+$ and $CD45^-$) as well as ILC1 (single cell, live, $EpCAM^-$ $CD45^+$, Lineage (CD3, CD5, CD19, Ly6G)$^-$, RORγt^-, $NKp46^+$, $KLRG1^-$ and $NK1.1^+$). SIO only controls (top) were FACS purified to ensure all cells experienced the same conditions prior to analysis, and to allow for flow quantification of epithelial CD44 (IM7). Additional ILC markers were included in the panel to confirm no significant loss of ILC1, and that no contaminating non-ILC1 cells (e.g. Lineage positive cells or RORγt+ cells), or differences in ILC1 cell-count existed between samples. Gates were set on FMOs for CD44, NKp46, and Lineage.

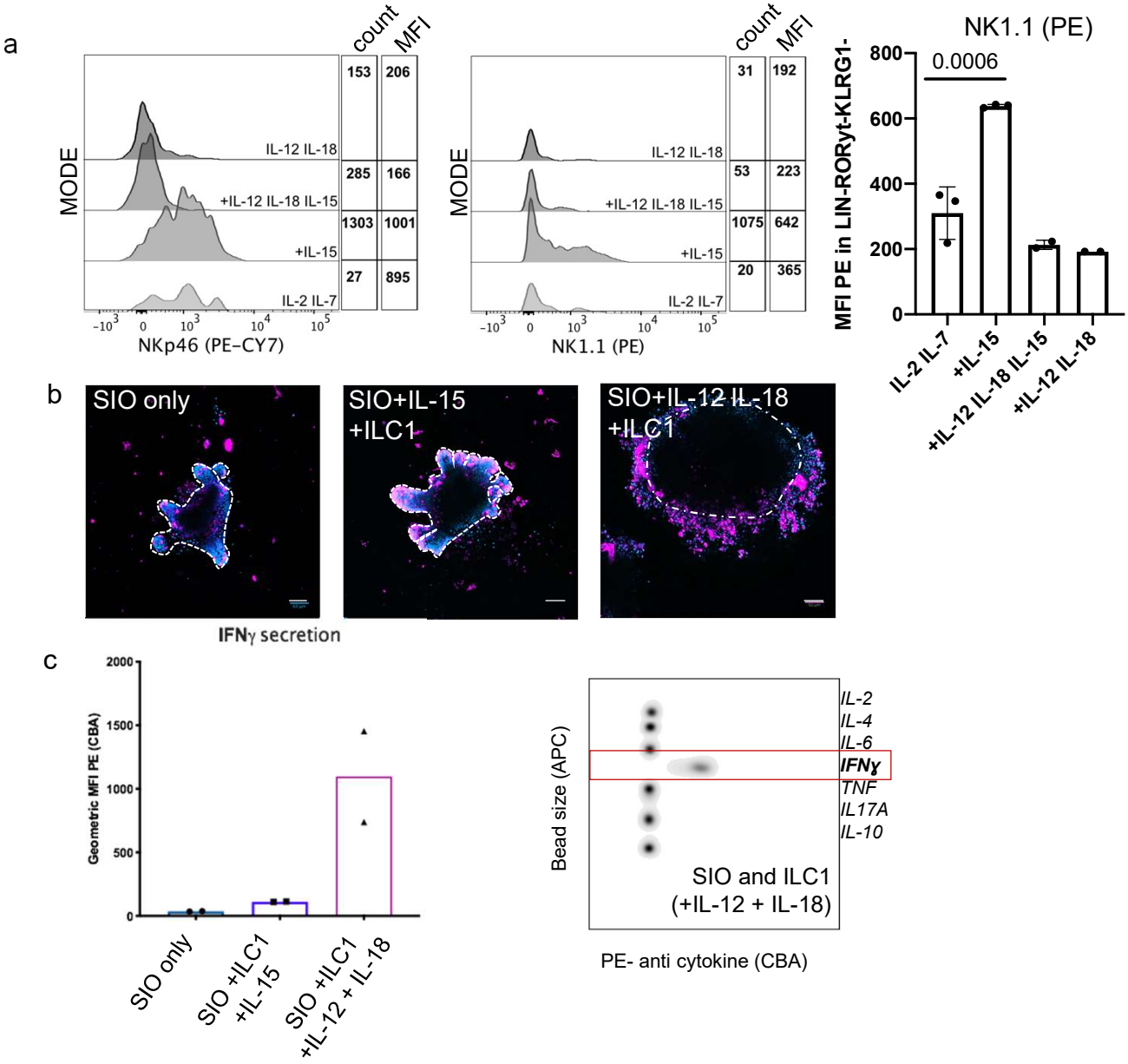

Supplementary Figure 3. Optimization of ILC1-SIO co-culture conditions

a) Representative modal histograms of NKp46 and NK1.1 mean fluorescence intensity (MFI) from EpCAM-CD45+Lin-KLRG1-RORyt- ILC1 following 4 days of co-culture with SIOs supplemented with IL-2, IL-7 and a combination of ILC1 polarizing cytokines. IL-12 and IL-18 reportedly drive plasticity of ILC3 and ILC2 to ILC1. However, in co-culture with SIOs, addition of these cytokines reduced characteristic natural cytotoxicity receptor (NCR: NKp46) and NK1.1 expression. The measured mean fluorescent intensity of NK1.1 and ILC1 count was highest in conditions supplemented with 0.2ng/ml IL-15.

X-axis = Mode (NK1.1 MFI) quantified in a OneWay ANOVA with Tukey's test shows significant difference between IL-2+IL-7 and IL-2+IL-7+IL-15 co-cultures, error bars S.E.M (ILC1 from N=3 separate mice, run in the same experiment).

b) Representative confocal images of 4 day ILC1-SIO co-cultures supplemented with either IL-15 or IL-12 and IL-18 show dramatic loss of SIO morphology indicative of potential loss in SIO viability in conditions with IL-12 and IL-18 with ILC1 (right). Scale bar 50µm.

c) Addition of IL-15 induces significant secretion of IFNγ. IL-12 and IL-18 increase IFNy expression, but not of other Th1/Th2/Th17 cytokines, as measured by flow Cytometric Bead Array (CBA), in which supernatant of co-culture was stained with APC-bead conjugated antibodies of different sizes, and then counterstained with PE-conjugated antibodies against cytokines, a method similar to an ELISA. Representative of co-cultures with ILC1 derived from 4 mice, pooled 2+2 (N=2).

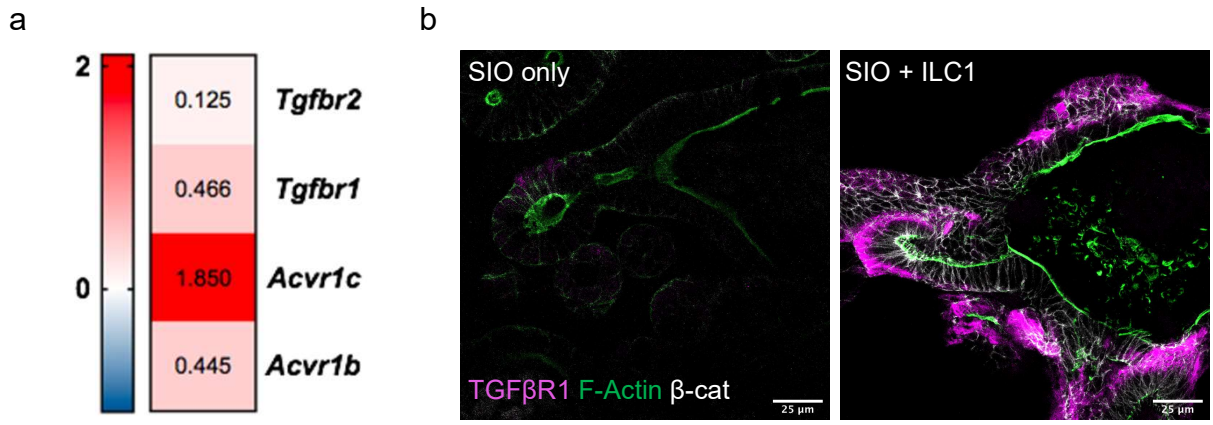

Supplementary Figure 4. Differential upregulation of TGFβR1 expression in SIO after co-culture with ILC1

a) Raw LogFC values of differentially expressed TGFβ Receptors upregulated in SIO epithelial cells after co-culture with ILC1 (red upregulated, blue downregulated in ILC1 co-cultures), extracted from RNAsequencing dataset (from ILC1 derived from N=3 separate mice): *Acvr1b* p=0.07; *Acvr1c* p=0.03; *Tgfbr1* p=0.03; *Tgfbr2* p=0.44, (p-values calculated using the markov chain monte carlo simulation with multiple testing correction performed using the Benjamini and Hochberg (1995) method).

b) Representative confocal image of SIO only and SIO+ILC1 showing TGFβR1 expression in magenta, F-actin in green, and β-catenin in white (Rep. of experiments with ILC1 from N=2 mice, scale bar 25µm.)

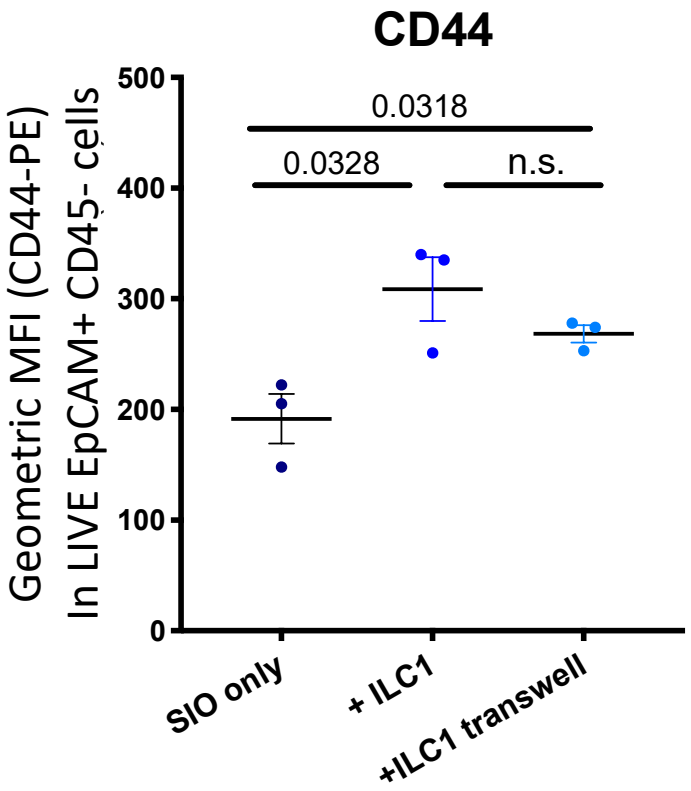

Supplementary Figure 5. ILC1 impact on IEC is not contact dependent
ILC1 separated from SIO by a transwell insert still drive significant upregulation of CD44 (IM7) MFI, as measured by flow cytometry in LIVE EpCAM+ CD45- cells. OneWay Anova with Tukey's test, ILC1 derived N=3 mice, separate experiments, error bars S.E.M.

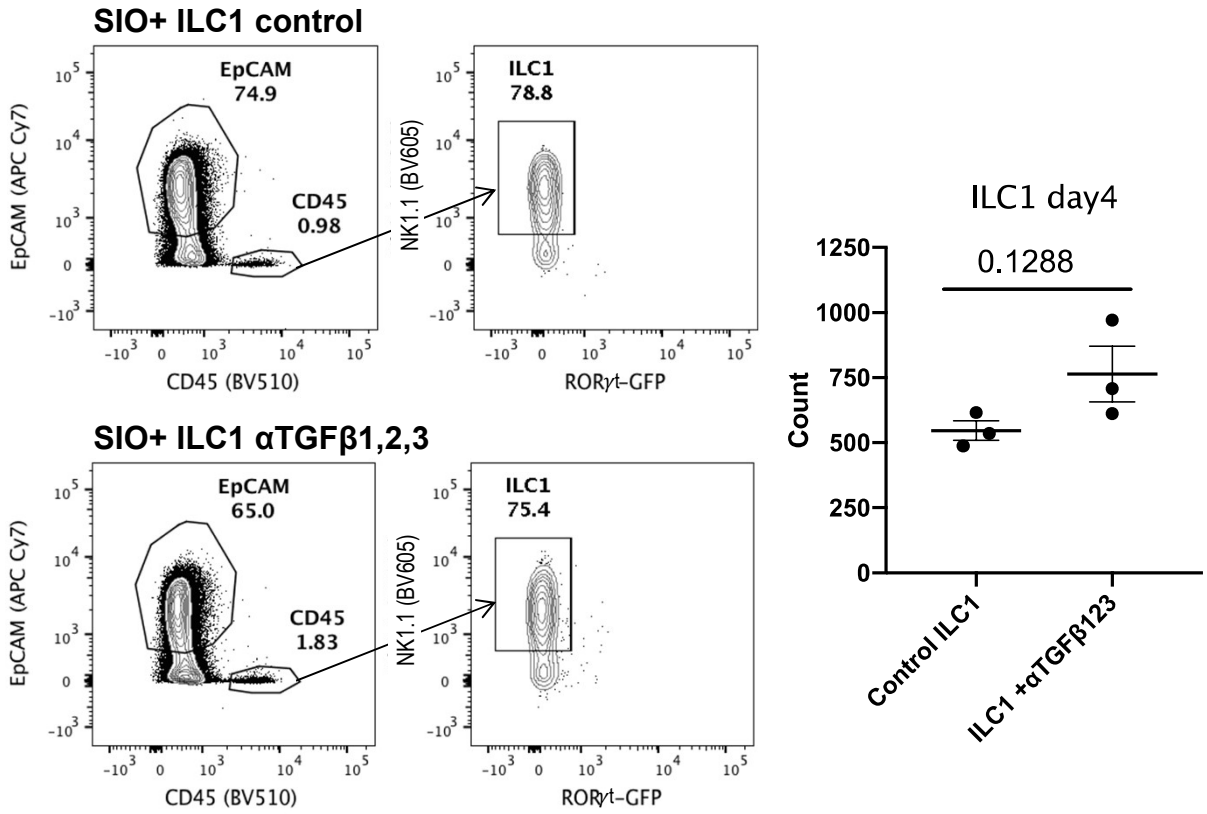

Supplementary Figure 6. TGFβ1,2,3 neutralization in ILC1-SIO cultures does not impact ILC1 phenotype

Representative plots from 4 day ILC1-SIO co-cultures with or without TGFβ1,2,3 neutralization (500 ng/ml) show that percentage of ILC1 (as defined in Supplementary Fig. 2) and count of LIVE, EpCAM-, CD45+, NKp46+, RORγt-, NK1.1+ ILC1 (ILC1 from N=3 individual mice) do not change significantly (Unpaired two-tailed student t-test, error bars S.E.M.), suggesting that any decrease in CD44 expression is not due to a loss of ILC1 phenotype or survival.

a

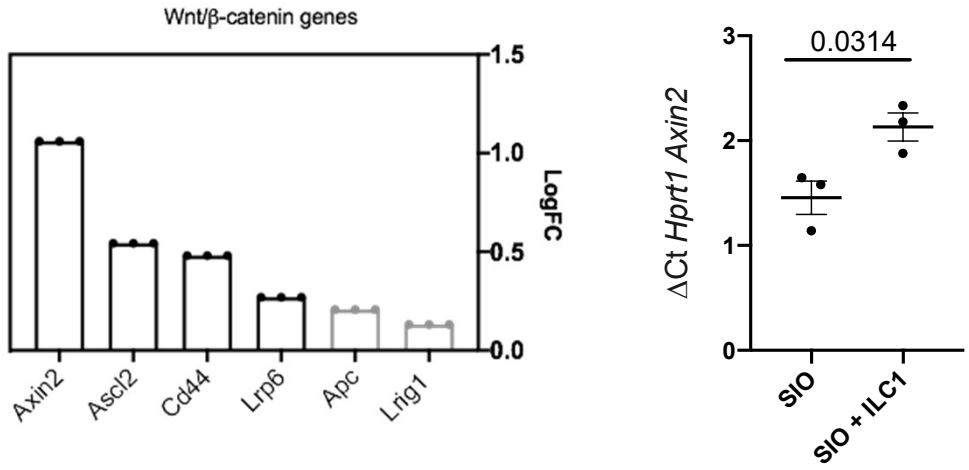

b

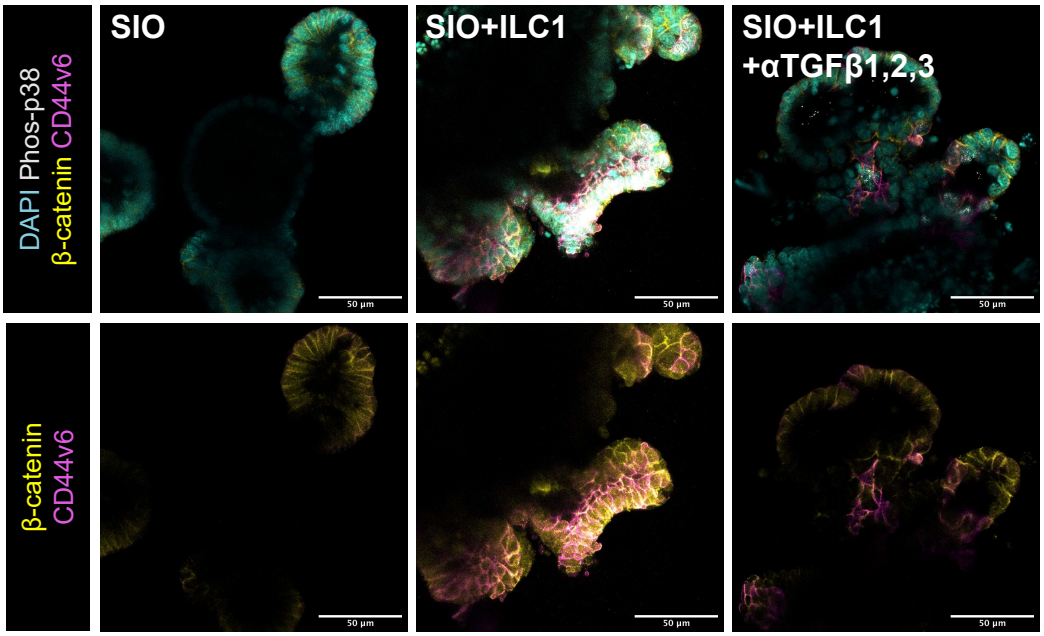

Supplementary Figure 7. ILC1 increase epithelial β-catenin expression
a) Raw logFC values extracted from the RNAsequencing dataset of genes of interest, involved in Wnt/β-catenin signaling in SIO + ILC1 cultures relative to SIO only controls on day4 (Boxes represent mean logFC of N=3 independent experiments with ILC1 from different mice, compiled in dataset1. Grey values are not statistically significantly differentially regulated (adjusted p>0.05. Axin2 p = 0.047; Ascl2 p = 0.047; Cd44 p = 0.008; Lrp6 p = 0.49; Apc p =0.85 Lrig1 p = 0.84;(p-values calculated using the markov chain monte carlo simulation with multiple testing correction performed using the Benjamini and Hochberg (1995) method)).
b) Additional images relating to Fig. 2g-i, with these images specifically showing co-staining of β-catenin (magenta) and CD44v6 (yellow) only, showing overlapping accumulation of both targets in the same regions/cells of the organoid (CD44v6 quantified in 2e, β-catenin quantified in Fig2i, ILC1 derived from N=3 separate mice). Scale bars 50µm.

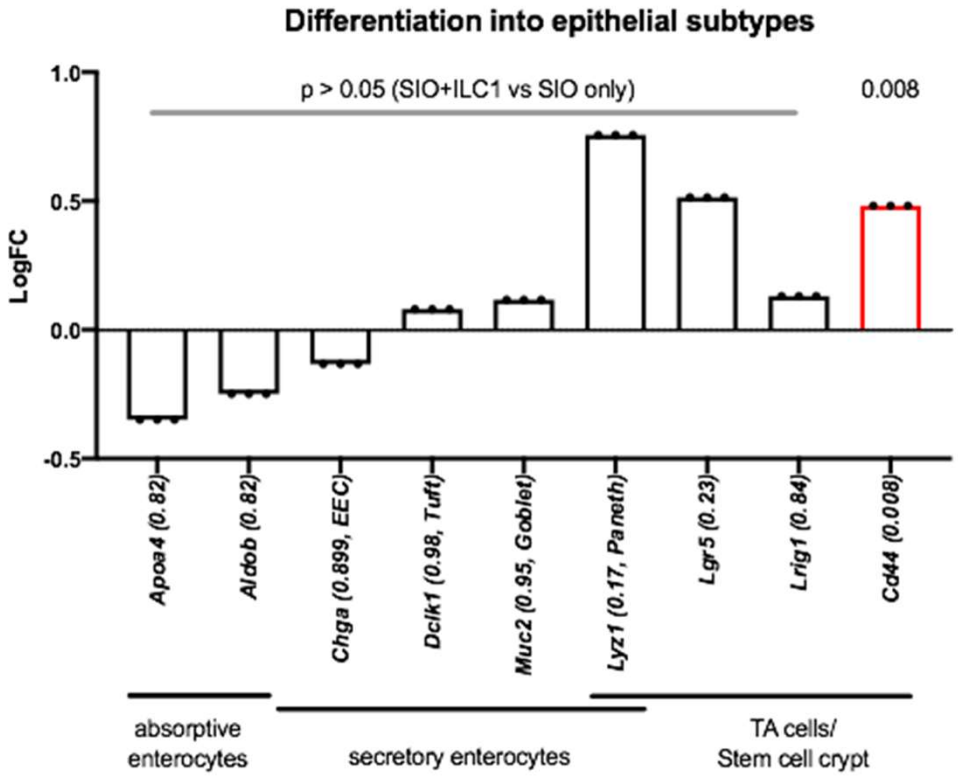

Supplementary Figure 8. ILC1 do not significantly alter IEC subset-specific gene expression
LogFc of differentially expressed genes in SIO+ILC1 relative to SIO only on day4, extracted from RNA-sequencing dataset (from ILC1 derived from N=3 separate mice) show no significant difference in key marker expression relative to SIO only control. Adjusted p-values indicated in brackets after gene names, along with the epithelial subtype they characterize (*Apoa4* p=0.82; *Aldob* p=0.82; *Chga* p-0.899; *Dclk1* p=0.98; *Muc2* p=0.95; *Lyz1* p=0.17; *Lgr5* p=0.84; *Lrig1* p=0.84; *CD44* p=0.008; (p-values calculated using the markov chain monte carlo simulation with multiple testing correction performed using the Benjamini and Hochberg (1995) method)).

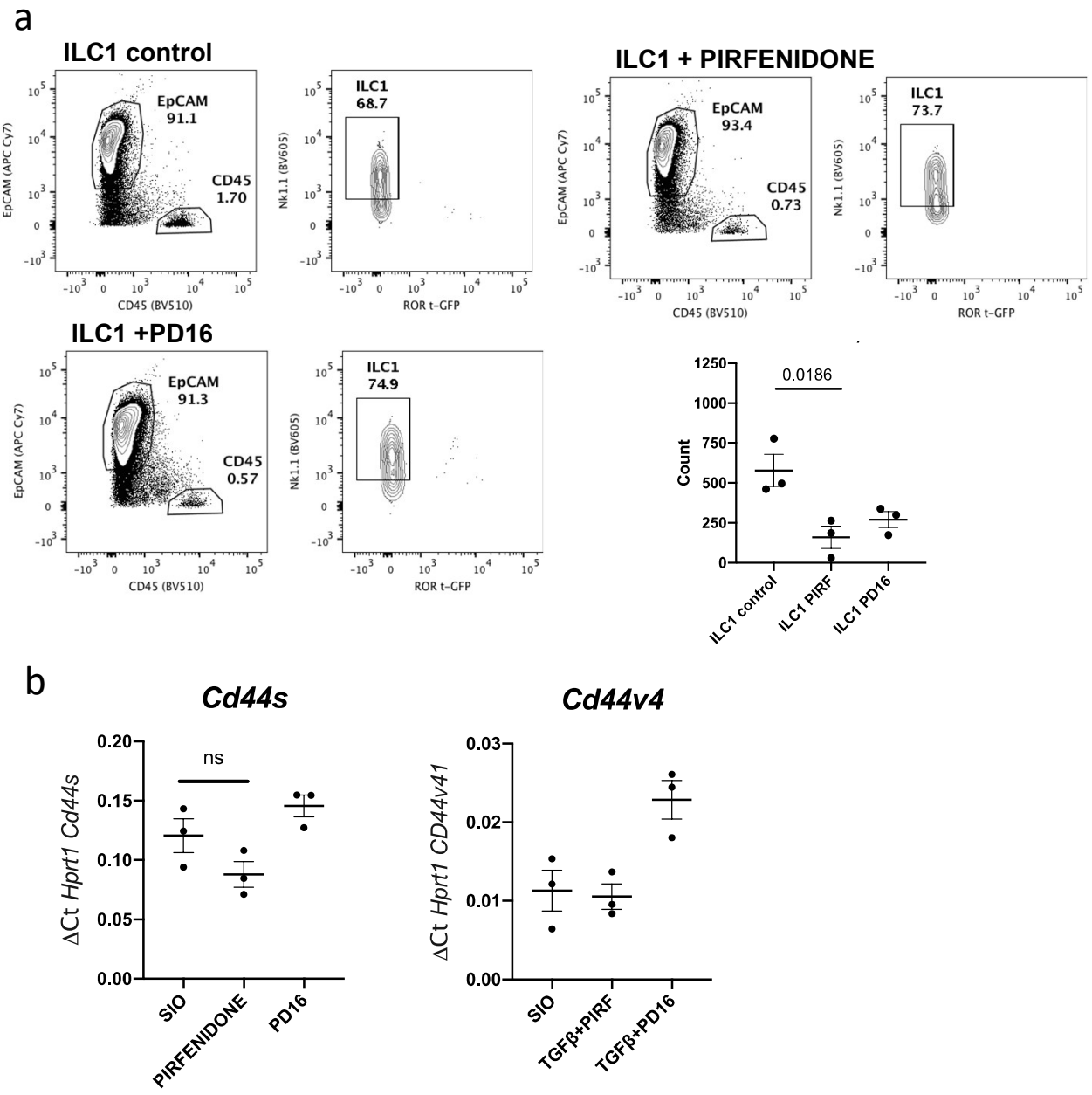

Supplementary Figure 9. Impact of p38 inhibition on ILC1 and on SIO

a) Representative FACS plots from 4 day ILC1-SIO co-cultures with regular IL-15 media or supplemented with Pirfenidone (50µM) or PD16 (5µM). While ILC1 phenotype itself was not significantly impacted, the number of ILC1 (count live, EpCAM- CD45+) after co-culture decreased significantly to below 250 cells/50000 recorded events (~2000 cells per condition). Count: OneWay ANOVA with Tukey's test of ILC1 co-cultures from N=3 mice. Error bars S.E.M.

b) RTqPCR of *Cd44s* and *Cd44v4* in SIO cultured with TGFβ1 alone, with Pirfenidone, or PD16 for 4days (relates to Figure 2k). Two-tailed student t-test between SIO and Pirfenidone in *Cd44s* condition show no significant difference in *Cd44s* or *Cd44v4* expression induced by Pirfenidone; Experiments performed with ILC1 from N=3 different mice. Error bars S.E.M.

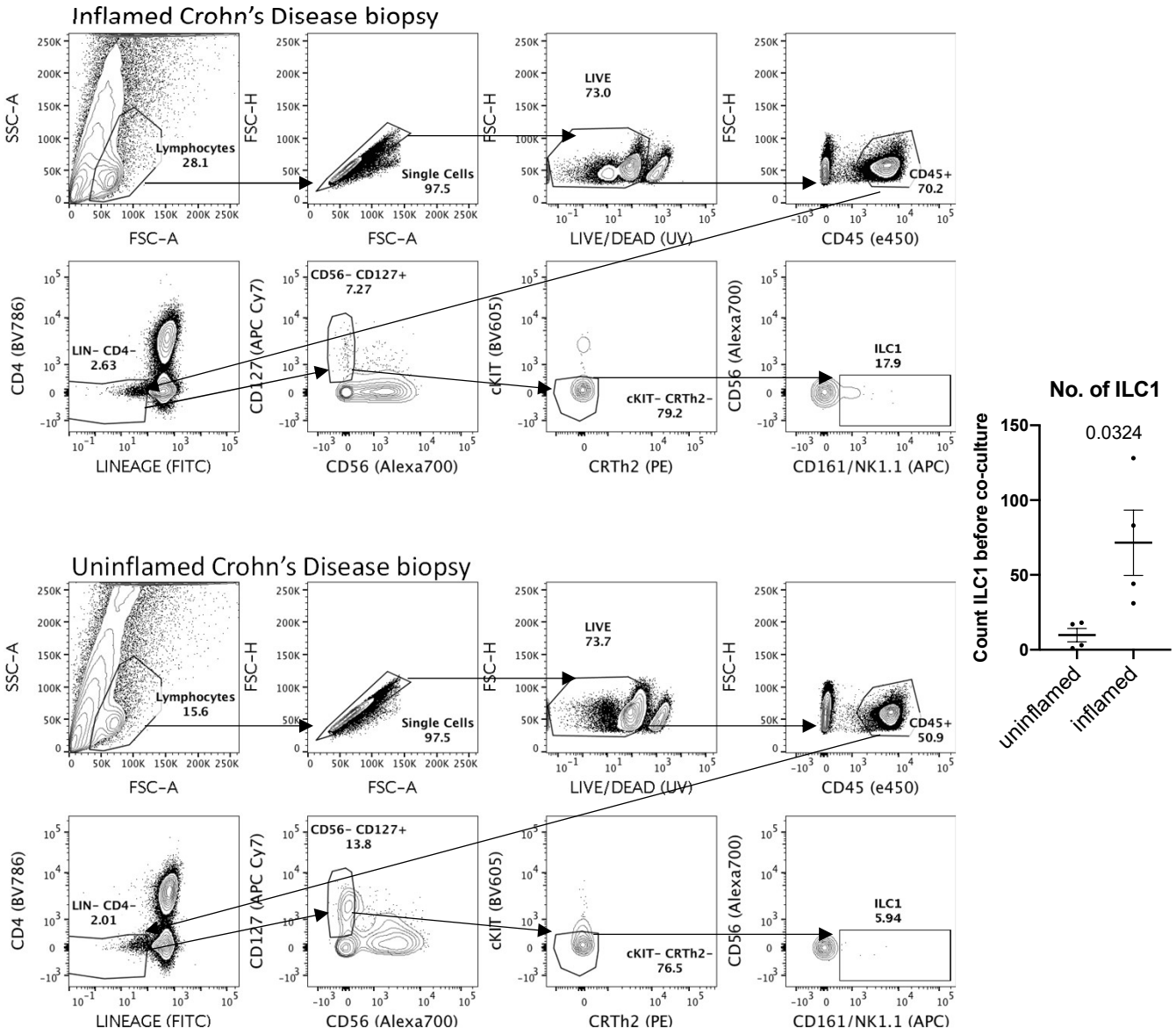

Supplementary Figure 10. Gating strategy for hILC1 from patient lamina propria biopsies
Colonic lamina propria ILC1 were purified from 15-18 biopsies of IBD (predominantly Crohn's Disease) patients with or without active inflammation. hILC1 were defined as LIVE, CD45+, CD4-, Lineage- (CD3, CD4, CD14, CD19, CD20, TCRαβ, TCR$\gamma\delta$), CD127+, CD56- (NK cells), cKIT- (ILC3 and precursors), CRTh2- (ILC2), CD161/NK1.1+. FACS plots representative of variation in hILC1 yield between patients, with a significant difference in ILC1 count from inflamed versus uninflamed (count of representative 100,000 events recorded during FACS, ILC1 derived from N=4 biopsies from uninflamed tissues and N=4 biopsies from inflamed tissues, performed in 8 individual experiments, unpaired two-tailed student t-test, error bars S.E.M.).

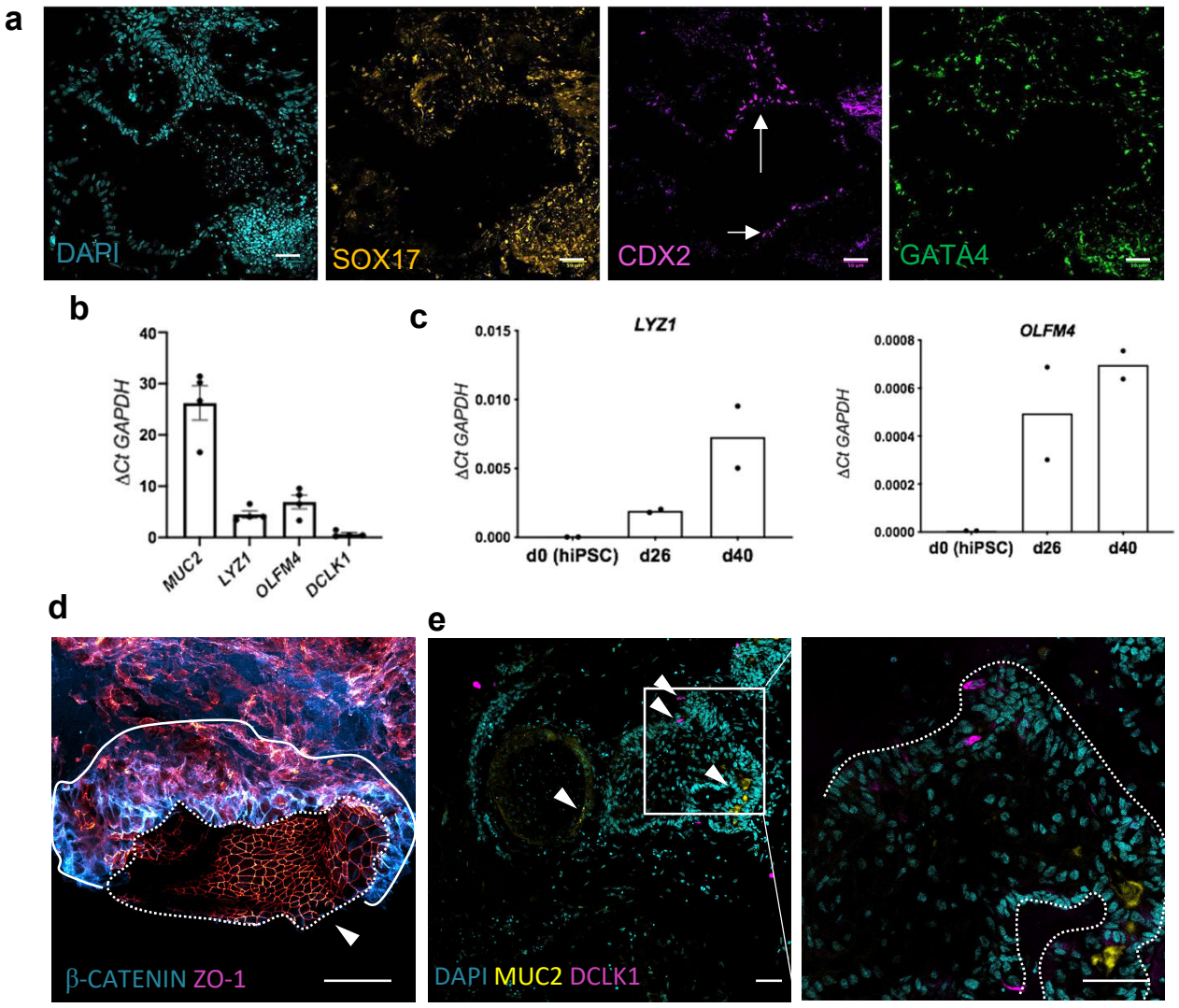

Supplementary Figure 11. Characterization of HIO development in Matrigel

a) Confocal images of representative of two independent experiments (separate differentiations) where 10 day old HIOs demonstrating characteristic definitive endoderm markers, with CDX2 expression restricted to the future epithelial buds that are picked and cultured in 3D Matrigel. Scale bar = 50µm.

b) HIO structures on express characteristic epithelial markers after 24 days of differentiation. Error bars represent S.E.M., values derived from N=2 rounds of differentation, with two technical replicates (two wells, n) per differentiation.

c) HIO show a trending increase in the expression of anti-microbial Paneth cell marker *LYZ1* and crypt cell marker *OLFM4* over the time course of differentiation (N=2 rounds of HIO differentiations, bars show the mean).

d) Confocal image demonstrating apico-basal expression of apical tight junction marker ZO-1, facing into the pseudolumen (indicated by white arrow, outlined in white dotted line), with β expression indicating organization in an epithelial structure in a d75 HIO. Scale bar = 50µm.

e) Confocal image representative of two independent experiments, and enhanced zoom of white box show that d75 HIO express markers of mature intestinal epithelium like Stem and Tuft cell marker DCLK1 (top white arrows) and deposition of mucous layer component MUC2 into the pseudolumen (yellow). Scale bar = 50µm.

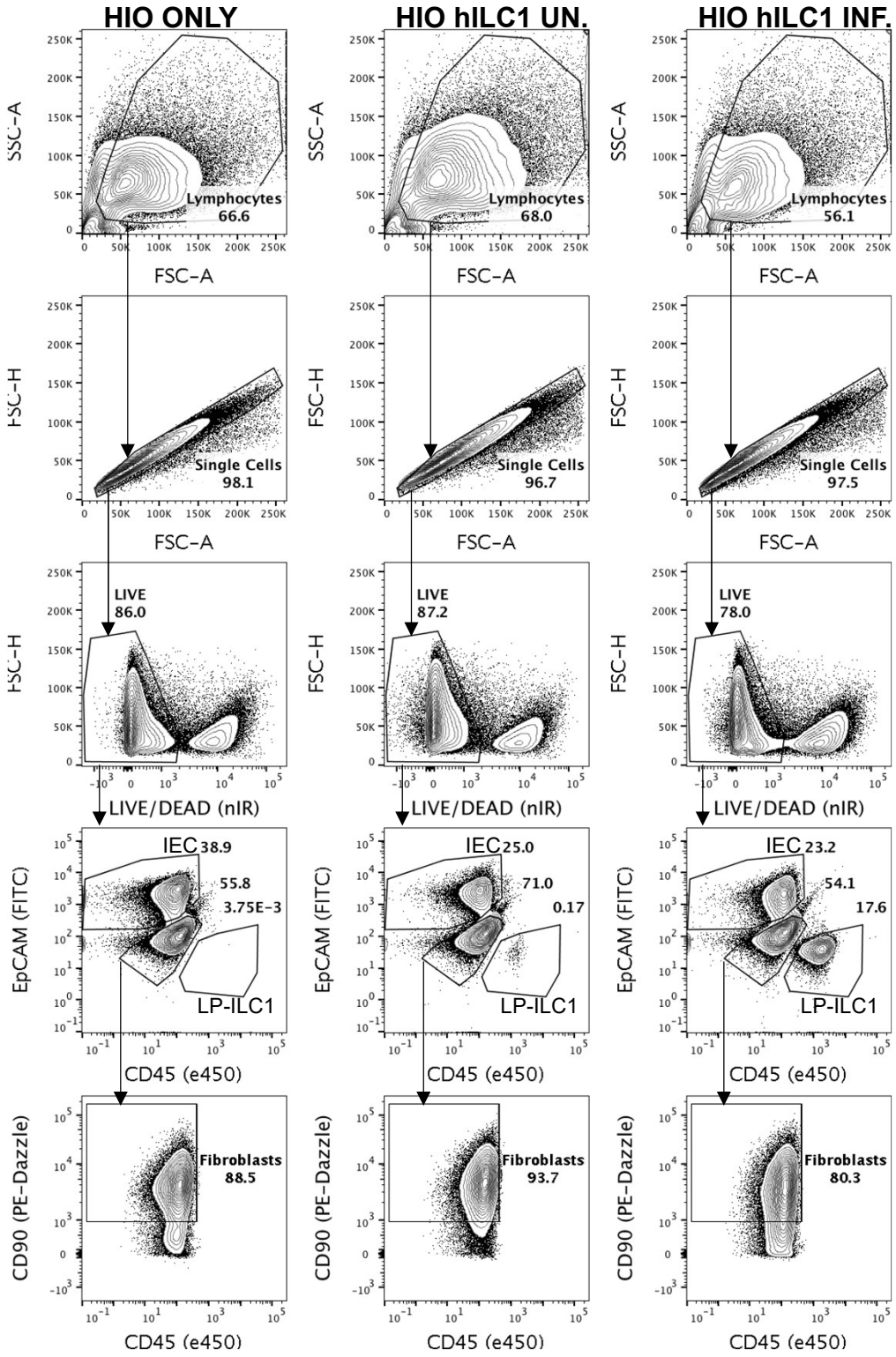

Supplementary Figure 12. HIO and hILC1 cell subtype FACS gating strategy after 7 day co-culture Epithelial cells from co-cultures were defined as single, live and $EpCAM^+$. Fibroblasts were defined as single cells, live, $EpCAM^-$, $CD45^-$ and $CD90^+$. hILC1 were defined as single cells, live, $EpCAM^-$, $CD45^+$

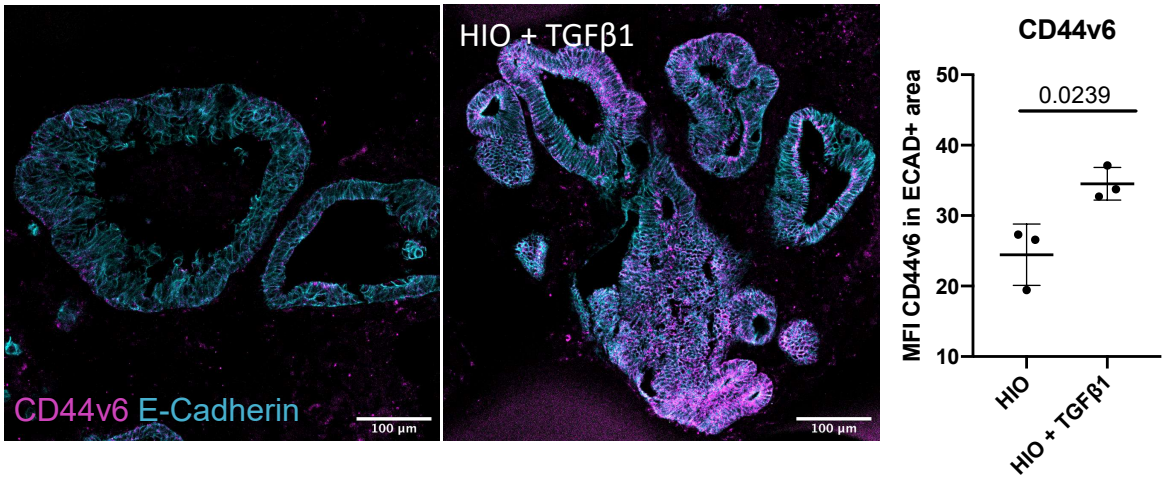

Supplementary Figure 13 TGFβ1 induces expression of CD44v6 in HIO

Representative confocal images CD44v6 (magenta) expression in HIO and HIO after 7 day co-culture with recombinant TGFβ1, with MFI of CD44v6 quantified in E-cadherin (cyan) regions (with HIO from N=3 rounds of differentiation). Scale bars 100µm. Two-tailed unpaired student t-test, error bars S.E.M.

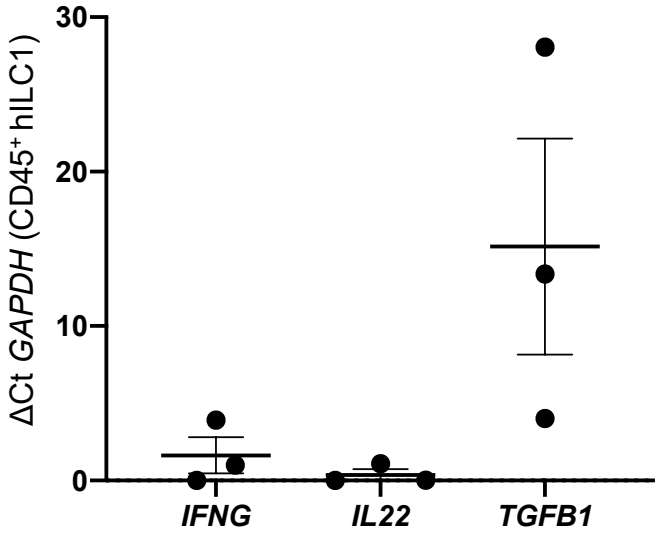

Supplementary Figure 14. hILC1 from inflamed IBD patients express *TGFB1*
Relative gene expression of *IFNG, IL22,* and *TGFB1* from activated uninflamed (N=1) and inflamed (N=2) patient biopsy derived hILC1 prior to co-culture. Error bars show the S.E.M..

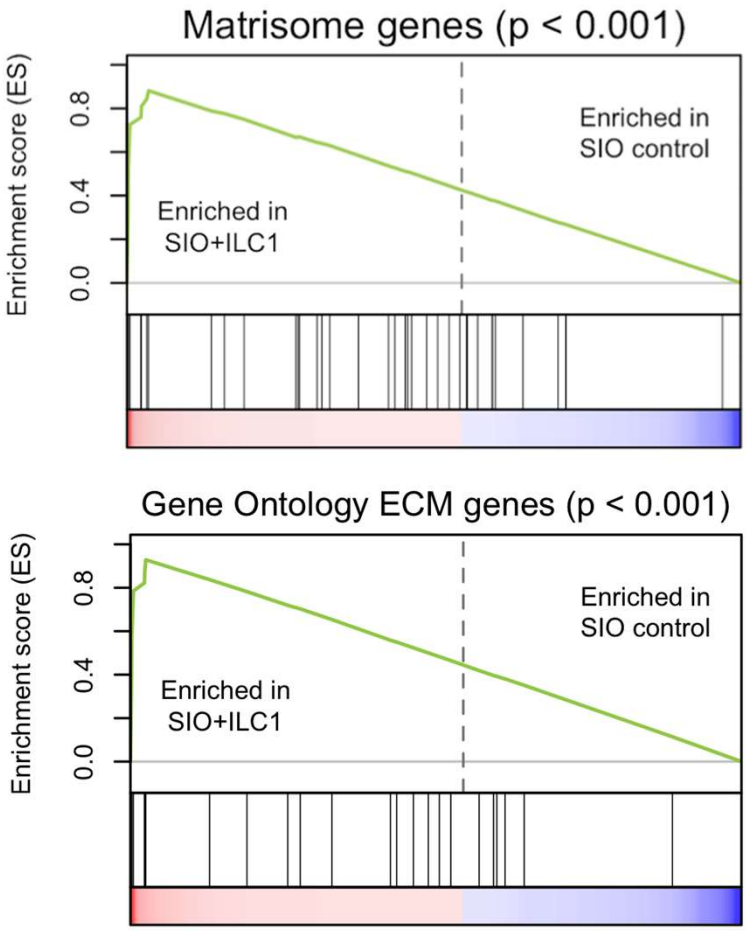

Supplementary Figure 15. GSEA analysis of murine RNA-sequencing shows enrichment of matrisome and ECM-associated genes in SIO co-cultured with ILC1 (From the RNA-sequencing dataset derived from co-culture of SIO with ILC1 from N=3 different mice; GSEA uses the non-parametric Kolmogorov-Smirnov test to assess p-values of gene set enrichment; $p < 0.001$ for Matrisome and ECM gene enrichment in ILC1 co-cultures)

.

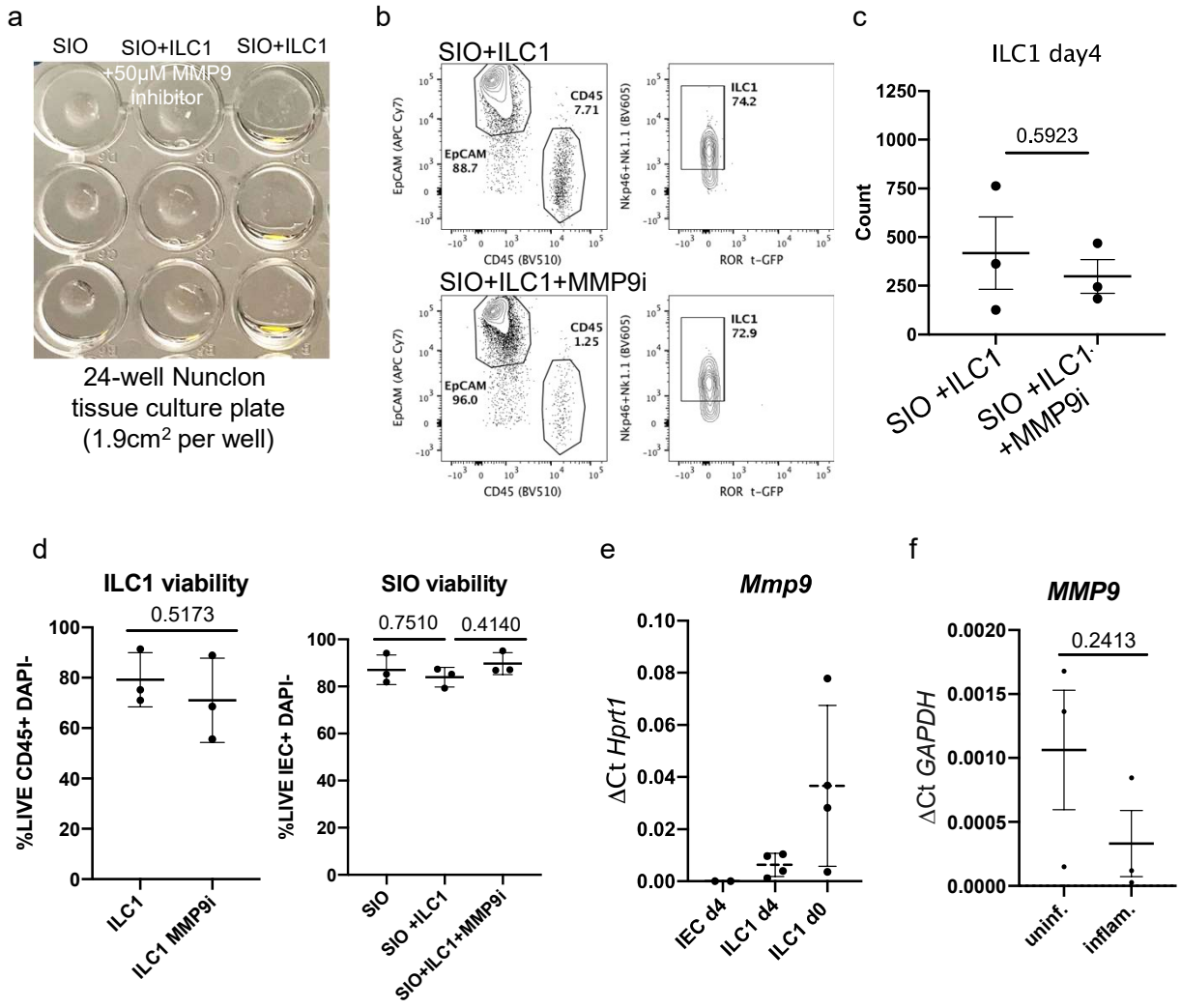

Supplementary Figure 16. ILC1 express MMP9 and drive Matrigel degradation

a) Image of Matrigel co-culture integrity after 24h with SIO only, SIO+ILC1+MMP9 specific inhibition (MMP9i), or SIO+ILC1 show complete degradation of Matrigel bubble in ILC1 co-cultures, reversible by MMP9i. SIO in SIO+ILC1 condition are pooled in PBS at the bottom of the well, or are loosely attached to the tissue culture plastic (Unpaired two-tailed t-test, ILC1 from N=3 mice).

b) Representative plots from day 4 ILC1-SIO co-cultures with MMP9 inhibition (50µM) show (c) no significant loss of ILC1 cell count due to MMP9i. Experiment repeated with ILC1 derived from N=3 mice, unpaired two-tailed t-test, error bars S.E.M.

d) Flow cytometry analysis of viability (DAPI) in CD45+EpCAM- ILC1 (left) and CD45-EpCAM+ IEC on day4 of co-culture with or without MMP9i Experiment repeated with ILC1 derived from N=3 mice, unpaired two-tailed t-test, error bars S.E.M.

e) *Mmp9* expression in murine ILC1 before (ILC1 derived from N=4 mice sorted directly into lysis buffer) and after (ILC1 from N=3 mice) co-culture with SIO, and in CD45-EpCAM+ IEC after co-culture. Unpaired two-tailed t-tests, error bars S.E.M

f) Relative expression of *MMP9* in human hILC1 from uninflamed (ILC1 derived from N=3 patients' biopsies) or inflamed patients (ILC1 derived from N=3 patients' biopsies) after 7 day co-culture with HIO. Unpaired two-tailed t-test, error bars S.E.M.

a

	System	PEG-4NPC	PEG-4VS	Peptides	Ions	Water
A_4+B_4	Ac-KDWERC-NH2	40	40	0	160 Na^+	533336
	H-SREWERC-NH2	40	40	0	0	533336
A_2+B_4	Ac-CREWERC-NH2	0	80	160	0	533336

b

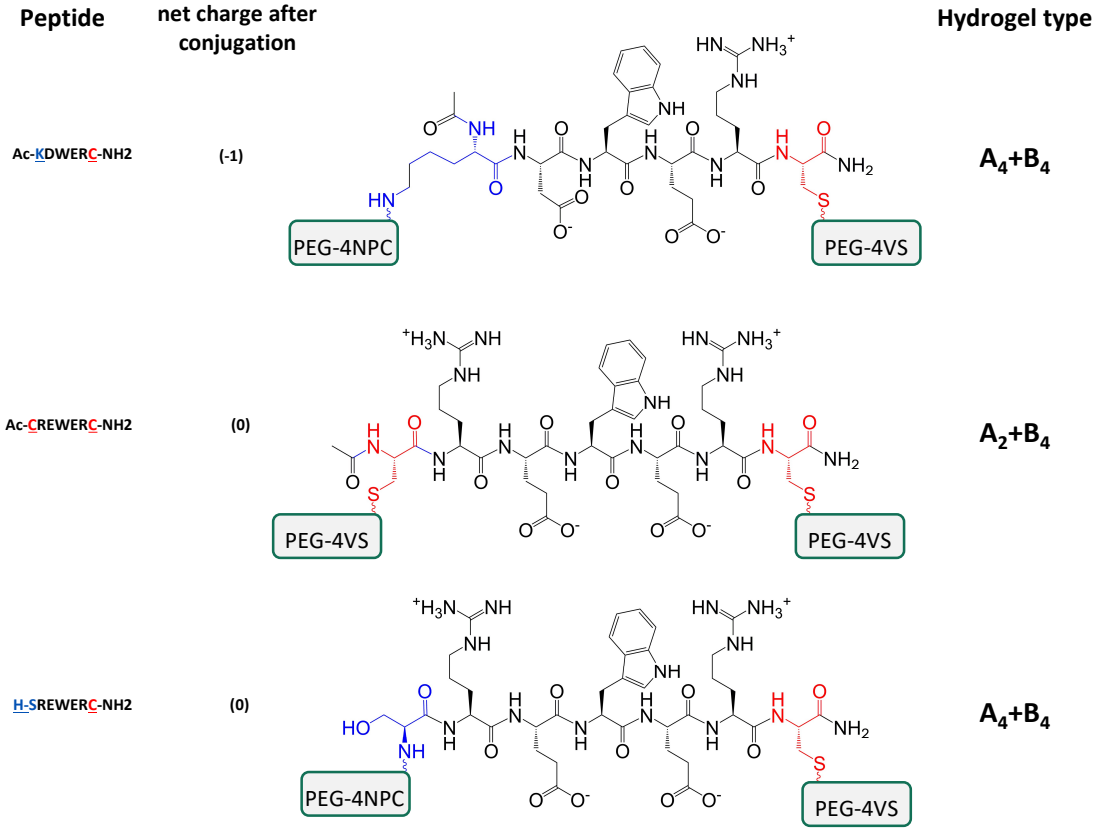

Supplementary Figure 17. Hydrogel systems simulated by molecular dynamics
a) Table outlining the systems characterized using molecular dynamics simulations with details on the number of pre-conjugated PEG-peptide molecules (PEG-4NPC), PEG molecules (PEG-4VS), free peptides, and ions in each simulation. The number of water beads was identical in each system and is 4 times the number of beads. Systems are designated by their cross-linking peptide. Simulations were run twice for each condition.
b) Chemical structure of peptides used in simulations. Peptide Ac-KDWERC-NH2was the non-adhesive/non-degradable peptide in our experimental hydrogel design (A_4+B_4). Simulations were also run with 'mutated' peptides H-SREWERC-NH2 and Ac-CREWERC-NH2.

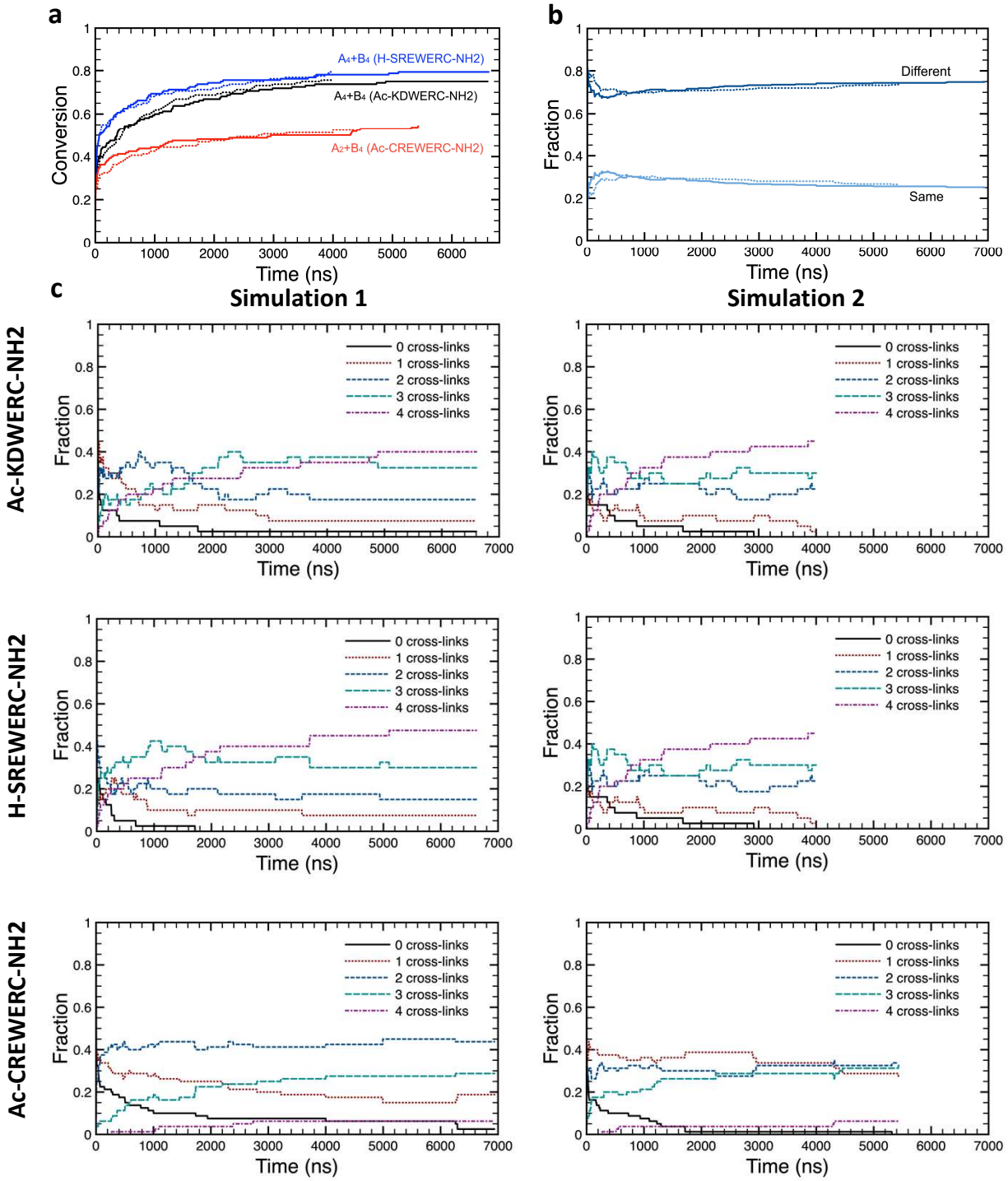

Supplementary Figure 18. Additional findings from molecular dynamics simulations

a) Fraction of total possible network forming bonds that form in simulated systems. Lines show two independent simulations per condition. The H-SREWERC-NH2 peptide forms 0.79 of possible network forming bonds.

b) Fraction of peptides in the A_2+B_4 design (Ac-CREWERC-NH2) that form two new bonds between arms of the *same* PEG molecule (primary loops) or between two *different* PEG molecules (cross-linking). These observations are in line with reported experimental observations of 1° loop formation in A_2+B_4 systems (Gu, Y. *et al., PNAS (*2017)). Bonds between arms of the same PEG molecule are precluded in simulations of the A_4+B_4 design.

c) Fraction of PEG molecules (PEG-4VS) that have formed 0, 1, 2, 3, or 4 network forming bonds (cross-links) as a function of time for the 3 different systems. As ~25% of bonds formed in the A_2+B_4 design (Ac-CREWERC-NH2) are not network forming, a larger fraction of PEG molecules form only 1 or 2 network forming cross-links, as opposed to the A_4+B_4 designs where the majority of PEG molecules form 3 or 4 network forming cross-links.

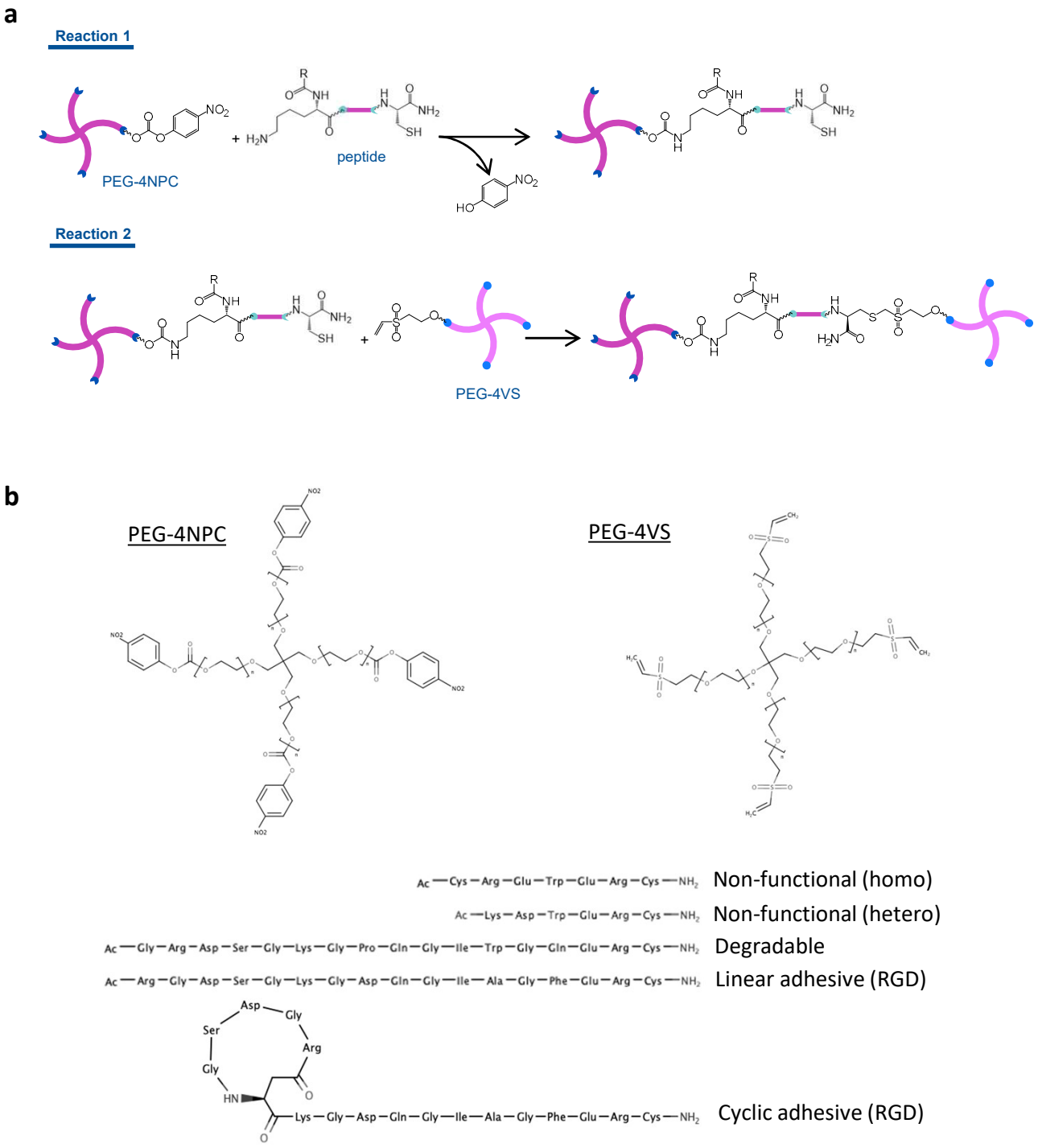

Supplementary Figure 19. Chemical strategy to form PEG-based hydrogels
a) Reaction schemes used to form hydrogels.
b) Chemical structures of PEGs and peptides used to form hydrogels. During peptide synthesis, the N-terminal amine was acetylated (or reacted with an aspartate side chain for cyclic adhesive RGD), rendering it non-reactive. Peptides were designed such that the degradable sequence is placed in between the peptide cross-linking points, i.e. between the lysine and cysteine residues, while the RGDS sequences are placed at the N-terminal and before the reactive lysines. In many A_2+B_4/B_8 designs, cell adhesive peptides are presented through a pendant chemical group that does not contribute to cross-linking, meaning that modulation of ligand concentration may result in concurrent unintended modulation of cross-linking and consequently stiffness. By rendering all peptides capable of cross-linking, our design ensures that ligand density can be modulated independently of stiffness.

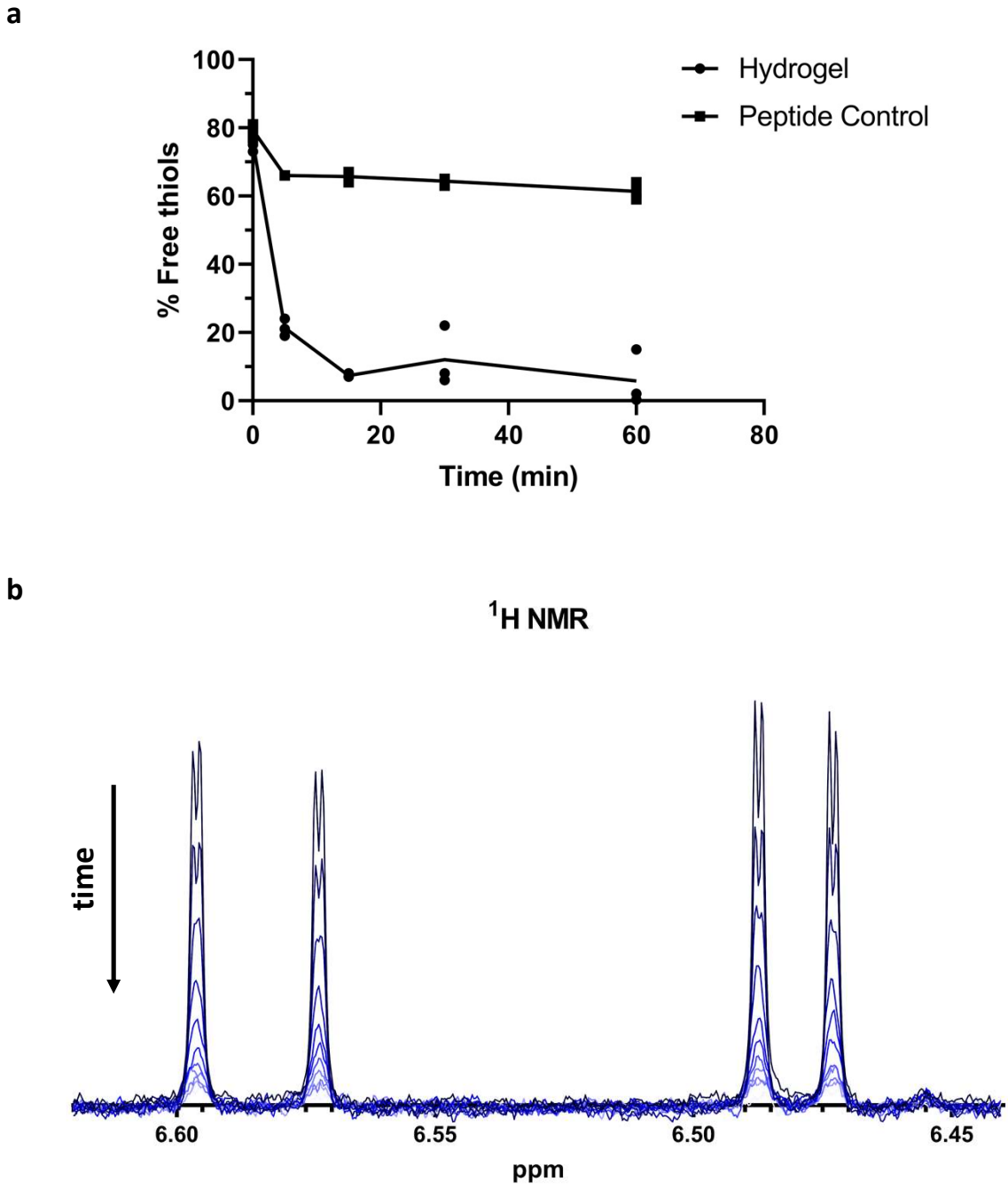

Supplementary Figure 20. Analysis of the efficiency of the click reaction used to form hydrogels
a) Plot showing the percent of total free thiols consumed during the Michael addition reaction to form hydrogels as determined by Ellman's assay. Nearly 80% of free thiols were consumed within 5 min and 94% within 1 hr. Lines connect mean values (N=3 independent hydrogels).
b) Proton NMR spectra showing the kinetics of the reaction over 60 min by monitoring the disappearance of olefinic vinyl bonds at 6.5841 (M=2, J1= 16.6000 Hz, J2= 0.8959 Hz) and 6.4800 (M=2, J1= 10.0440 Hz, J2= 0.9131 Hz) ppm as a result of the Michael addition. Within 6 min, 70% of the vinyl groups had disappeared, and 99% were gone after 60 min. Lines are coloured lighter as time proceeds.

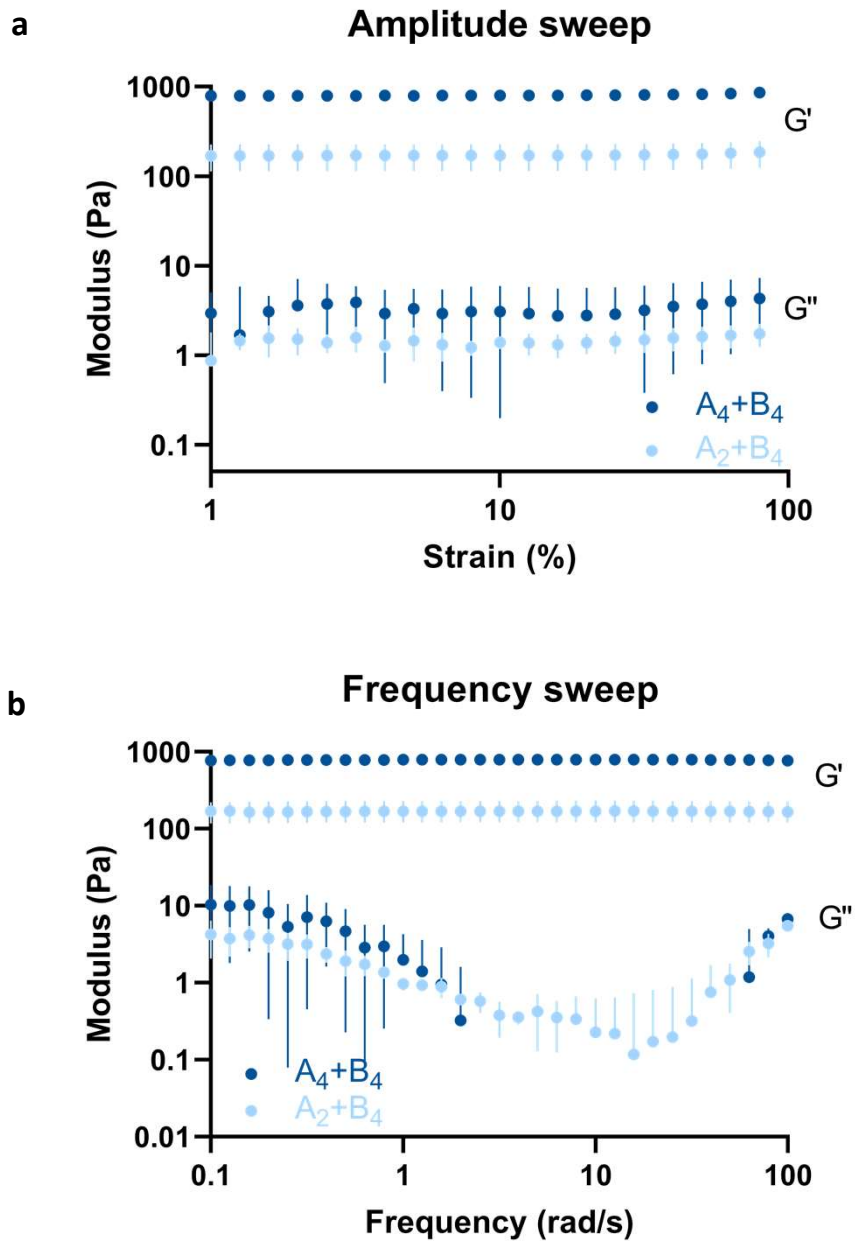

Supplementary Figure 21. Rheological characterization of A_4+B_4 and A_2+B_4 hydrogels
a) Mean values of G' and G'' obtained using amplitude sweeps on A_4+B_4 and A_2+B_4 hydrogels (N=3 independent hydrogels, error bars show S.D.).
b) Mean values of G' and G'' obtained using frequency sweeps on A_4+B_4 and A_2+B_4 hydrogels (N=3 independent hydrogels, error bars show S.D.).
For some values of strain and frequency, G'' for A_4+B_4 hydrogels could not be obtained. Taken together with the time sweep measurements (Fig. 4e), these data suggest that A_4+B_4 hydrogels have a higher elastic modulus, behave more elastically, and are more reproducible (less inter-sample variability) than A_2+B_4 designs.

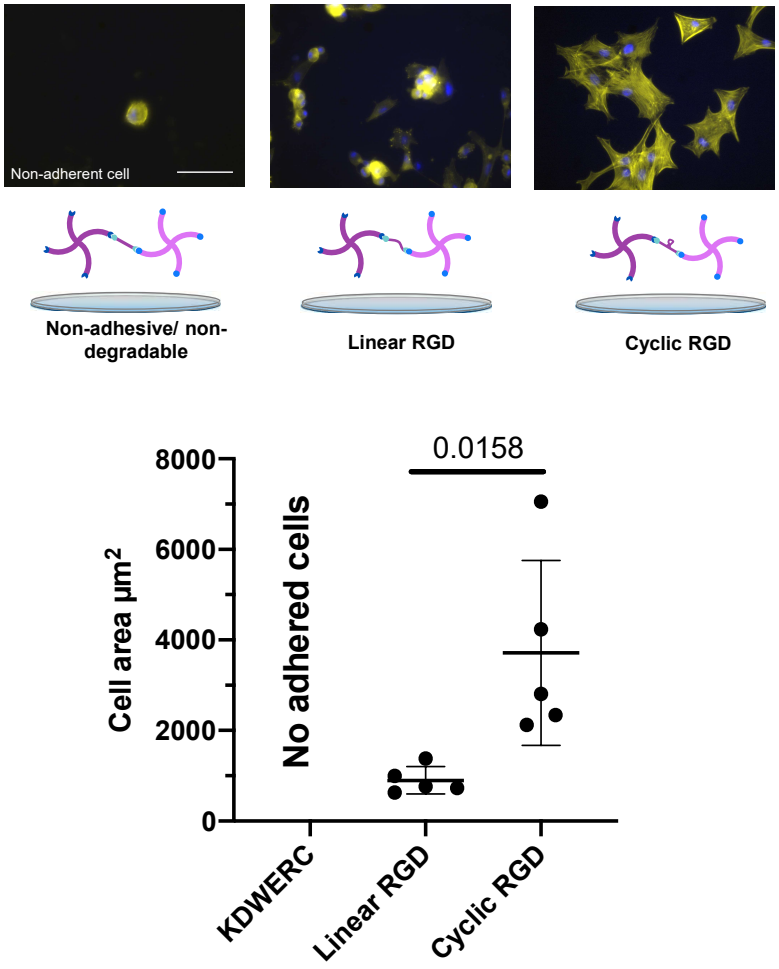

Supplementary Figure 22. hMSC adherence on 2D hydrogel surfaces
Representative fluorescence micrographs of hMSC cultured on 2D hydrogels stained with phalloidin-TRITC and DAPI (1 experiment per condition). hMSC do not adhere to hydrogels formed with non-adhesive/non-degradable peptides. On hydrogels formed with a linear RGD sequence, hMSC display a mixture of round and spread morphologies, but when all peptides contain a cyclic RGD sequence, hMSC adopt highly spread morphologies. Unpaired two-tailed t-test between Linear RGD and Cyclic RGD, error bars S.E.M. (N=5, cells per condition) Scale bar = 50µm.

a

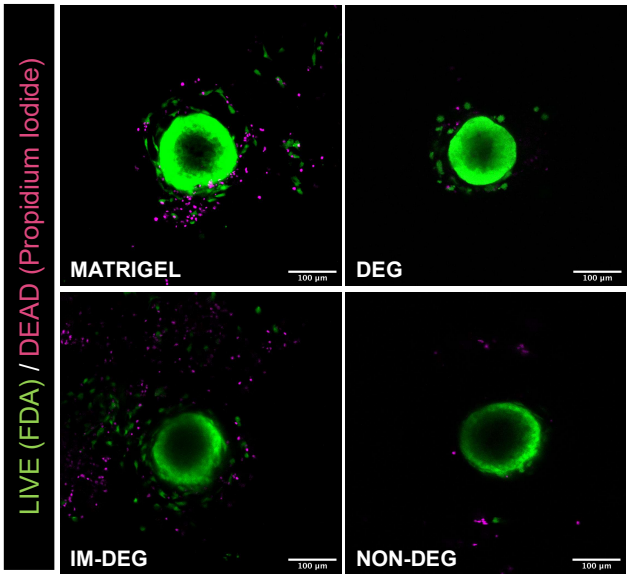

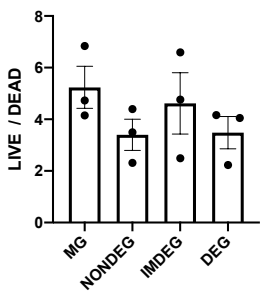

Tukey's multiple comparisons test	95.00% CI of diff.	Summary	Adjusted P Value
MG vs. NONDEG	-1.973 to 5.651	ns	0.4571
MG vs. IMDEG	-3.188 to 4.435	ns	0.9509
MG vs. DEG	-2.053 to 5.570	ns	0.4916
NONDEG vs. IMDEG	-5.027 to 2.596	ns	0.7426
NONDEG vs. DEG	-3.892 to 3.732	ns	0.9999
IMDEG vs. DEG	-2.676 to 4.947	ns	0.7781

b

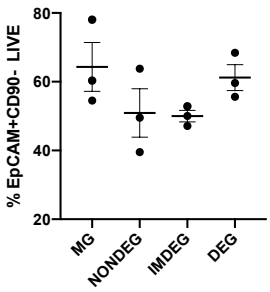

Tukey's multiple comparisons test	95.00% CI of diff.	Summary	Adjusted P Value
DEG vs. IMDEG	-13.30 to 35.70	ns	0.4989
DEG vs. MG	-27.64 to 21.37	ns	0.9753
DEG vs. NONDEG	-14.24 to 34.77	ns	0.5647
IMDEG vs. MG	-38.84 to 10.17	ns	0.3103
IMDEG vs. NONDEG	-25.44 to 23.57	ns	0.9993
MG vs. NONDEG	-11.10 to 37.90	ns	0.3604

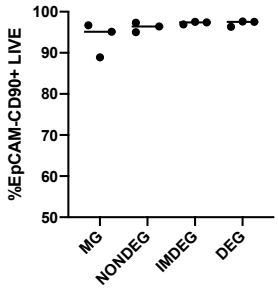

Tukey's multiple comparisons test	95.00% CI of diff.	Summary	Adjusted P Value
DEG vs. IMDEG	-5.823 to 5.557	ns	0.9998
DEG vs. MG	-2.123 to 9.257	ns	0.2616
DEG vs. NONDEG	-4.790 to 6.590	ns	0.9552
IMDEG vs. MG	-1.990 to 9.390	ns	0.2372
IMDEG vs. NONDEG	-4.657 to 6.723	ns	0.9349
MG vs. NONDEG	-8.357 to 3.023	ns	0.4797

Supplementary Figure 23. Viability of HIO in different hydrogel compositions

a) Representative confocal images (max projection of 5 z-stacks) of HIO from 3 rounds of differentiation (~day45) after culture in Matrigel, DEG (75% MMP-degradable), IM-DEG (45% MMP-degradable), or NON-DEG (0% MMP-degradable) hydrogels and FIJI quantification of Live/Dead normalized MFI from N=3 rounds of differentiation (error bars S.E.M., OneWay ANOVA with Tukey's post-hoc test, padj n.s.).
b) Flow cytometry of fixable Live/Dead staining (nearInfraRed/APC-Cy7, ThermoFischer) of HIO in Matrigel (MG), or encapsulated in NON-DEG, IM-DEG, or DEG hydrogels from N=3 rounds of differentiation (~day45) show no significant differences in viability between Matrigel and any hydrogel condition in CD90-EpCAM+ IEC, or in CD90+EpCAM- Fibroblasts (error bars S.E.M., OneWay ANOVA with Tukey's post-hoc test, padj n.s.).

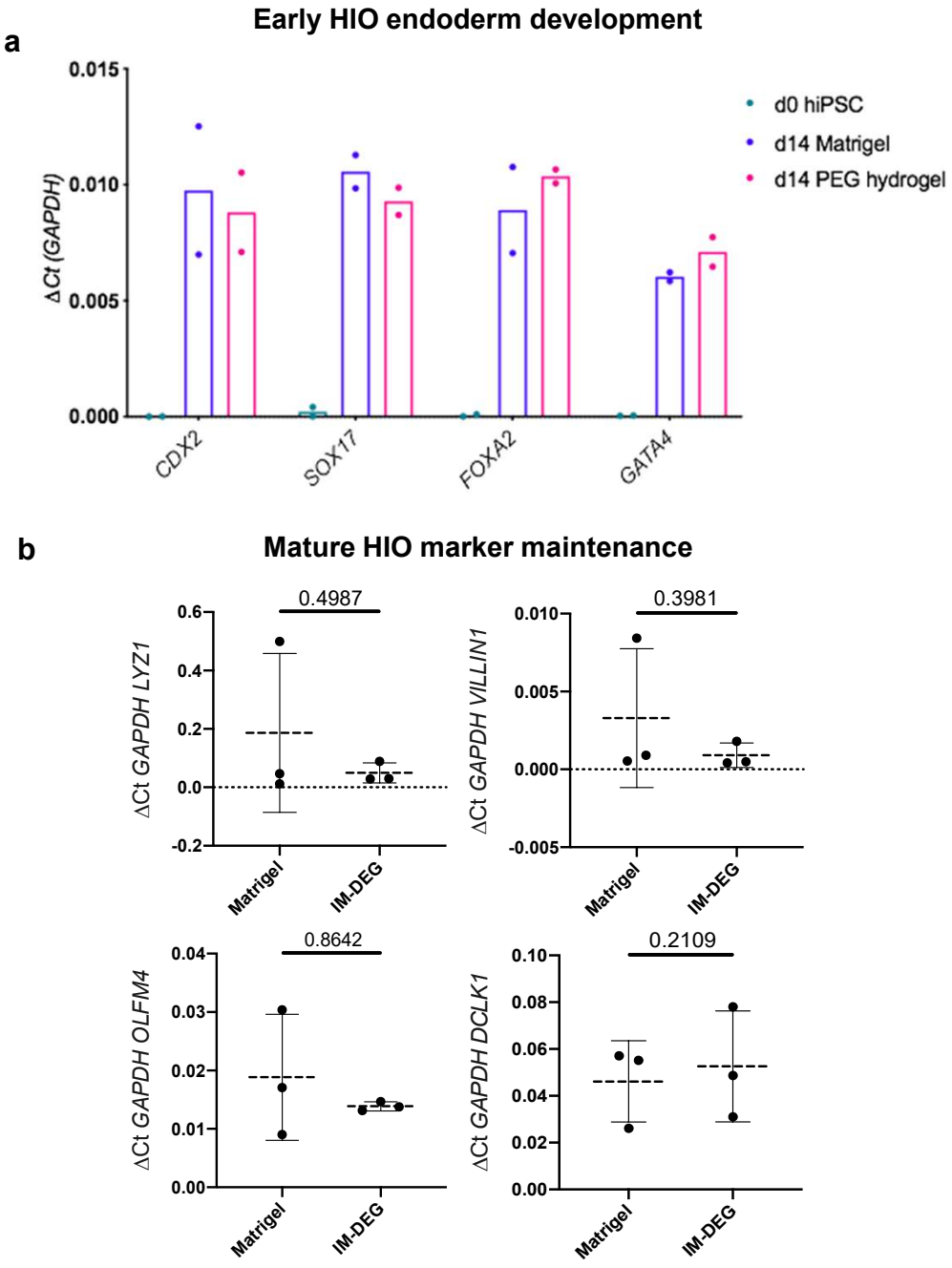

Supplementary Figure 24. Characterization of human induced pluripotent stem cell (hiPSC)-derived human intestinal organoids (HIOs) in novel synthetic hydrogel system

a) Expression of endodermal markers (*CDX2*, *SOX17*, *FOXA2* and *GATA4*) is significantly upregulated between day 0 hiPSC and d14 differentiated immature HIO, but not different between HIOs cultured in Matrigel versus IM-DEG PEG hydrogel at day 14, suggesting maturation into hindgut endoderm organoid fate is not adversely affected by PEG hydrogel culture (from N=2 separate HIO differentiations, bars show the mean).

b) Relative expression of mature gut markers in d75 HIO cultured in Matrigel or post 7-day encapsulation in IM-DEG hydrogel show no significant differences in expression of *OLFM4* (stem cell), *LYZ1 (Paneth Cell), VILLIN1 (Enterocyte), or DCLK1 (Tuft cell).* Unpaired two-tailed t-tests, error bars show S.E.M.

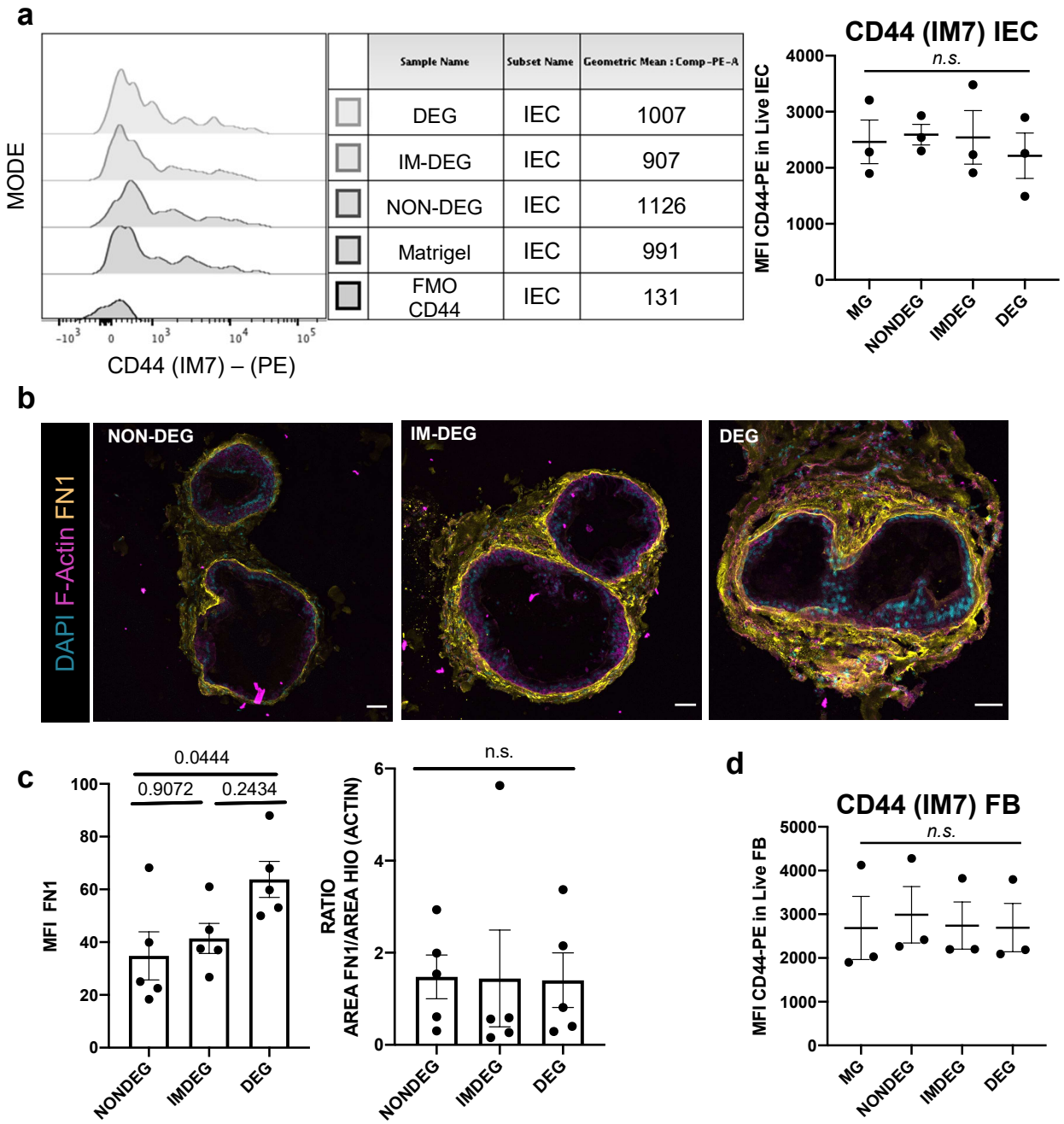

Supplementary Figure 25. Proposed hydrogel is a suitable system for ECM remodelling studies

a) Representative MFI of CD44-PE from flow cytometry of HIO-derived IEC (EpCAM+, CD90-) with quantification (right) show that IEC do not alter their levels of CD44 expression in IM-DEG gels relative to Matrigel, and that CD44 expression is not impacted by degradability of the surrounding hydrogel (Error bars S.E.M., N=3 rounds of differentiation, ~d45; Oneway ANOVA with Tukey's post-hoc test, padj=n.s. for all values).

b) Representative confocal images of HIO in NON-DEG, IM-DEG, and DEG hydrogels show that HIO have the capacity to deposit ECM (Fibronectin1) in the synthetic hydrogel system, making it an appropriate model for further studies of matrix remodeling with aILC1. Scale bars 50μm, z-projection of 10 stacks.

c) FIJI quantification of FN1 deposition reveals that more FN1 is deposited in 75% DEG hydrogels than in 0% NON-DEG hydrogels (padj=0.0444, OneWay ANOVA, Tukey's post-hoc test, error bars S.E.M, N=5 HIO regions), however the area of deposited matrix is not significantly different between the same conditions.

d) HIO-derived fibroblasts (hFB) do not alter their levels of CD44 expression in IM-DEG gel, and CD44 expression is not impacted by degradability of the surrounding hydrogel (Error bars S.E.M., N=3 rounds of differentiation, ~d45; Oneway ANOVA with Tukey's post-hoc test, p*adj*=n.s. for all values)

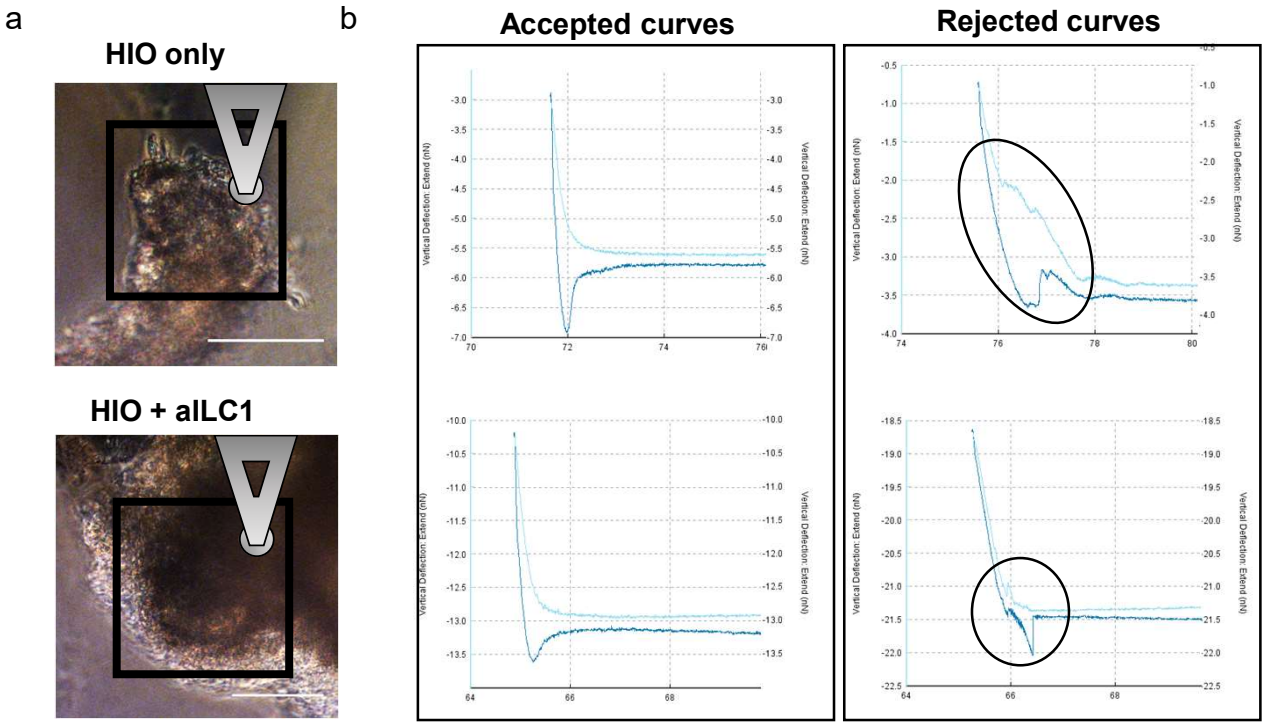

Supplementary Figure 26. AFM force maps collected on HIO-laden hydrogels

a) Force-distance curves were collected in maps on gels with encapsulated HIO with or without aILC1, with HIO regions determined through morphology in bright field images. Scale bar=100µm. Boxes highlight areas mapped in examples shown in Fig. 5b (HIO only/HIO+aILC1), and overlaid cartoons show the position of the cantilever. This experimental approach combined with the Hertzian model allows for the measurement of relative changes in *E* produced by experimental conditions. This is because although the AFM probe (bead d=50µm) only indents a small distance into the hydrogel surface, underlying soft/stiff hydrogel/secreted matrix will contribute to the material's mechanical response, akin to a "two-spring system", the concept of which is well described in the field of mechanics. In short, when a mechanical load is applied to two springs, with spring constants k1 and k2 in series, the mechanical response of the system will be a combination of both springs' mechanical properties. Here, k1 and k2 can be considered akin to the mechanical properties of the overlying hydrogel and underlying degraded hydrogel/secreted matrix. Such effects have been experimentally verified using AFM-based force spectroscopy measurements on microglial cells cultured on soft polyacrylamide substrates, whereby indentation measurements collected on the overlying cells were impacted by deformation of the underlying soft substrate, which impacted calculations of *E*. (Rheinlaender *et al., Nat Mater* (2020)[1])
b) Example force-distance curves collected during AFM-based stiffness mapping. Force curves were accepted if they had both a smooth clear indentation and a flat baseline (left). Curves for which it was apparent that the indentation had been disrupted (right) were rejected and are presented as crosses (X) on the stiffness maps.

[1]Rheinlaender, J., Dimitracopoulos, A., Wallmeyer, B. *et al.* Cortical cell stiffness is independent of substrate mechanics. *Nat. Mater.* (2020). https://doi.org/10.1038/s41563-020-0684-x

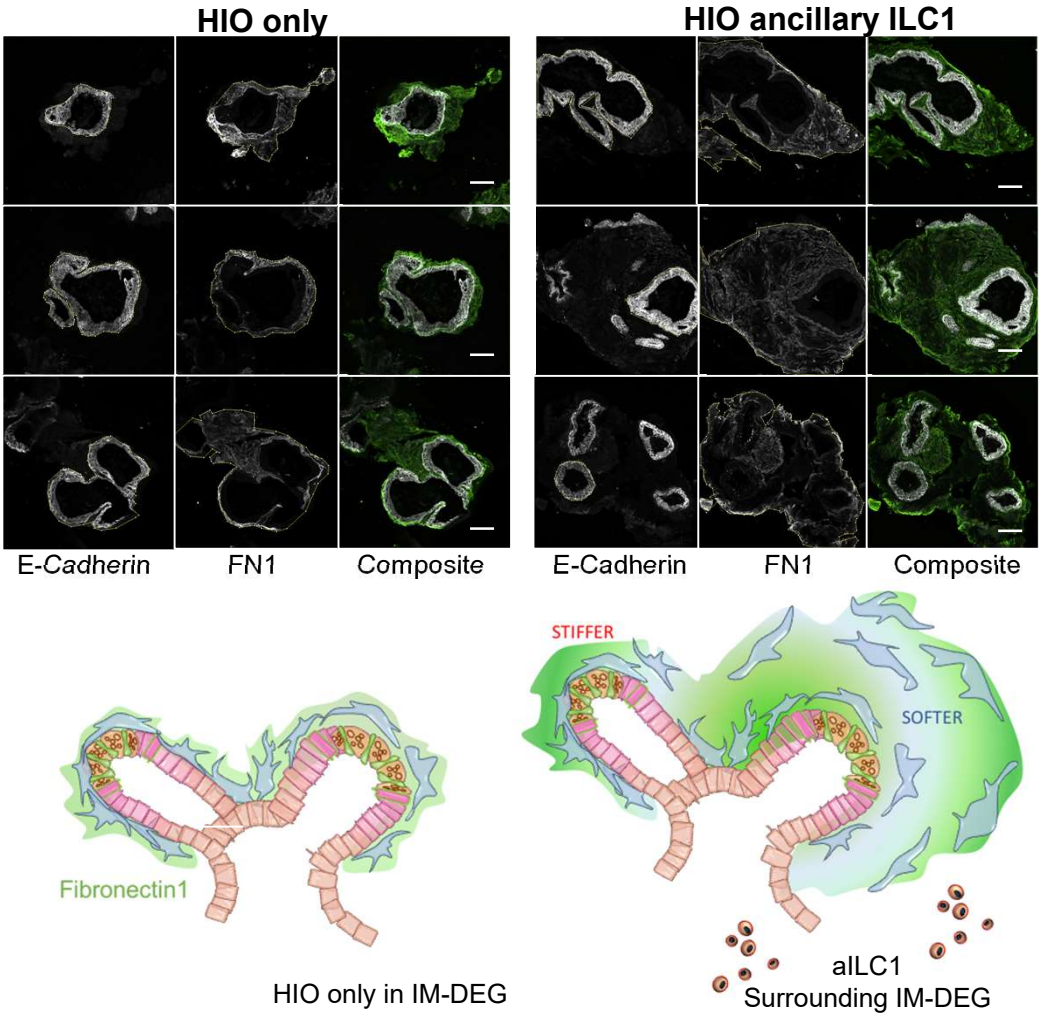

Supplementary Figure 27. Fibronectin deposition around HIO in IM-DEG hydrogels

Additional representative images of HIO in IM-DEG hydrogels after 4day co-culture either with (right) or without (left) ancillary ILC1. After AFM measurements were taken, HIO gels were PFA fixed and cryosectioned (14µm slices) and co-stained for E-cadherin (white) and Fibronectin1 (FN1, green). The outline of the E-CAD+ epithelial organoid and the edge of the FN1+ remodeled area (green) were detected by binary mapping in FIJI, and the FN1+ area was subtracted from the E-CAD+ area to normalize for the size of the epithelial organoid (N=5 separate organoid areas per condition) to show the relative area of ECM remodelling (relates to Fig. 5g). Scale bars 100μm.

Diagrams beneath each condition represent the differential FN1 deposition (green) and matrix softening allowing for fibroblast to spread out (blue, softer, aILC1 condition) but also depositing FN1, making fibroblast-dense regions stiffer (dark green).

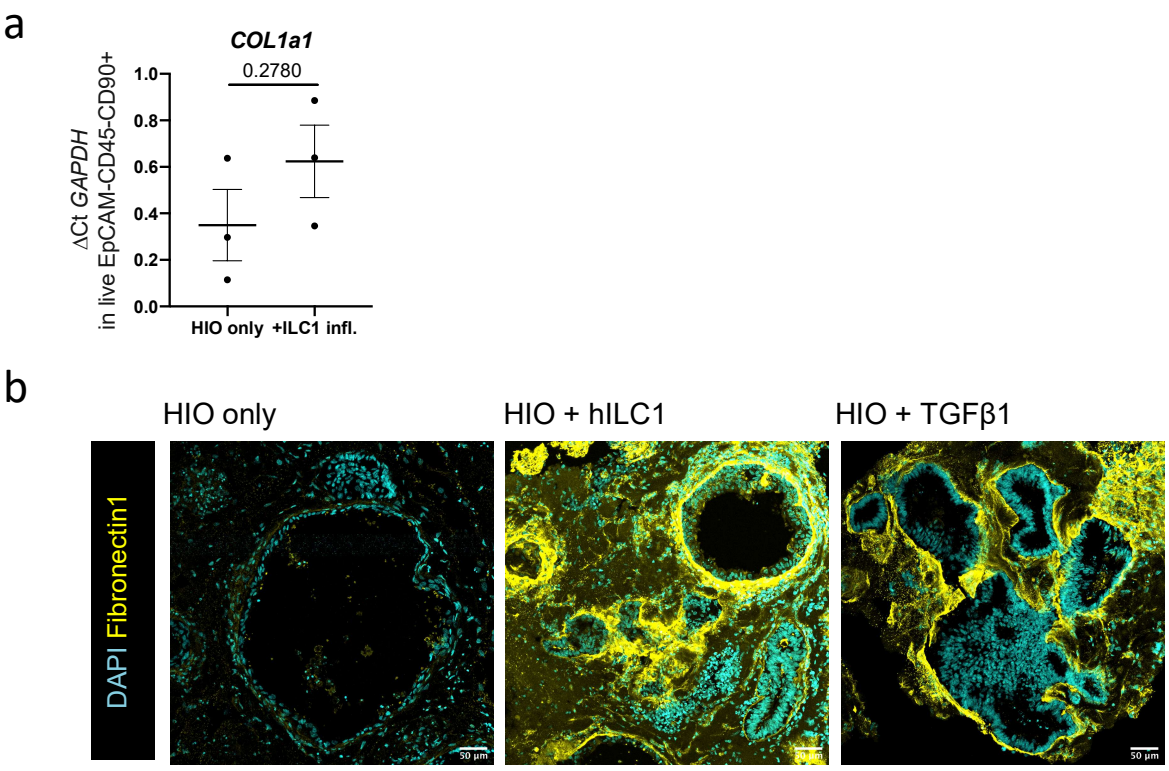

Supplementary Figure 28. *COL1a1* gene expression and fibronectin deposition around HIO in Matrigel

a) RTqPCR of *COL1a1* expression in HIO-derived fibroblasts with or without hILC1 co-culture from inflamed tissue biopsies. Two-tailed student t-test, error bars represent S.E.M of N=3 experiments from ILC1 derived from different inflamed patient biopsies.
b) Representative confocal images of HIO cultured alone, with hILC1, or with addition of recombinant TGFβ1 after 7days in Matrigel (Rep. of N=2, max projection of 10 stacks in each condition, scale bars 50μm).